Excited state quantum phase transitions
in many-body systems

M.A. Caprio [a,*], P. Cejnar [b,c], F. Iachello [a]

[a] *Center for Theoretical Physics, Sloane Physics Laboratory, Yale University, New Haven, CT 06520-8120, USA*
[b] *Institute of Particle and Nuclear Physics, Faculty of Mathematics and Physics,*
Charles University, V Holešovičkách 2, 180 00 Praha, Czech Republic
[c] *European Centre for Theoretical Studies in Nuclear Physics and Related Areas, Strada delle Tabarelle 286,*
38050 Villazzano (Trento), Italy

Abstract

Phenomena analogous to ground state quantum phase transitions have recently been noted to occur among states throughout the excitation spectra of certain many-body models. These excited state phase transitions are manifested as simultaneous singularities in the eigenvalue spectrum (including the gap or level density), order parameters, and wave function properties. In this article, the characteristics of excited state quantum phase transitions are investigated. The finite-size scaling behavior is determined at the mean-field level. It is found that excited state quantum phase transitions are universal to two-level bosonic and fermionic models with pairing interactions.
© 2007 Elsevier Inc. All rights reserved.

PACS: 03.65.Fd; 03.65.Sq; 64.60.−i

1. Introduction

Quantum phase transitions (QPTs), or singularities in the evolution of the ground state properties of a system as a Hamiltonian parameter is varied, have been extensively studied for various many-body systems (e.g., Refs. [1–3]). Recently, analogous singular behavior

---

has been noted for states throughout the excitation spectrum of certain many-body models [4–10], namely the Lipkin model [11] and the interacting boson model (IBM) for nuclei [12]. These singularities have been loosely described as "excited state quantum phase transitions" (ESQPTs) [9]. In this article, we more closely and systematically examine the characteristics of such excited state singularities as phase transitions, to provide a foundation for future investigations. It is found that excited state quantum phase transitions occur in a much broader class of many-body models than previously identified.

Ground state QPTs are characterized by a few distinct but related properties. The QPT occurs as a "control parameter" ξ, controlling an interaction strength in the system's Hamiltonian $\hat{H}(\xi)$, is varied, at some critical value $\xi = \xi_c$. For specificity, we take the Hamiltonian to have the conventional form $\hat{H}(\xi) = (1 - \xi)\hat{H}_1 + \xi\hat{H}_2$. At the critical value: (1) The ground state energy E_0 is nonanalytic as a function of the control parameter at $\xi = \xi_c$. (2) The ground state wave function properties, expressed via "order parameters" such as the ground state expectation values $\langle\hat{H}_1\rangle_0$ or $\langle\hat{H}_2\rangle_0$, are nonanalytic at $\xi = \xi_c$. These two properties are not independent, since the evolution of the ground state energy and that of the order parameters are directly related by the Feynman–Hellmann theorem [13], which gives $dE_0/d\xi = \langle\hat{H}_2\rangle_0 - \langle\hat{H}_1\rangle_0$. (3) The gap Δ between the ground state and the first excited state vanishes at $\xi = \xi_c$. (Here we consider only *continuous* phase transitions. More specifically, the systems considered in this article undergo second-order phase transitions, in which discontinuity occurs in the second derivative of the ground state energy and the first derivatives of the order parameters.) Singularities strictly only occur for an infinite number of particles in the many-body system, but precursors can be observed even for very modest numbers of particles. For finite particle number N, the defining characteristic of the QPT is therefore not the presence of a true singularity but rather well-defined scaling behavior of the relevant quantities towards their singular large-N limits [14].

For the systems which exhibit *excited state* QPTs, the vanishing gap between the ground state and first excited state at the ground state QPT does not occur in isolation. Rather, there is a bunching of levels near the ground state, that is, a vanishing of the average level spacing $\bar{\Delta}$ or an infinite local level density $\rho \equiv \bar{\Delta}^{-1}$. The infinite level density, moreover, propagates to higher excitation energy (as illustrated for a two-level fermionic pairing model in Fig. 1) as the order parameter is varied from ξ_c, hence the concept of a continuation of the QPT to excited states. The singular level density occurs simultaneously with singularities in other properties of the excited states $|k\rangle$, such as the level energy E_k and the expectation values $\langle\hat{H}_1\rangle_k$ and $\langle\hat{H}_2\rangle_k$.

First, we review the essential properties of the two-level pairing many-body models, for both bosonic and fermionic constituents (Section 2). We find that ESQPTs are universal to these models, suggesting that the ESQPT phenomena may be broadly relevant, at least to systems dominated by pairing interactions. The semiclassical analysis of a "sombrero" potential provides a basis for understanding many of the properties of the quantum many-body ESQPT [6,9]. The semiclassical analysis of Refs. [6,9] is extended in Section 3 to address several properties relevant to the definition of phase transitions. In particular, the singularity in the eigenvalue spectrum and the finite-size scaling behavior for the ESQPT are determined at the mean-field level. Numerical calculations for the full quantum problem are considered in Section 4, where we investigate manifestations of the ESQPT in the excitation spectrum and in the properties of "order parameters" for the excited states. Finally, we consider the ESQPT as a boundary between qualitatively distinct "phases" (Section 5). The relationship between the U($n + 1$) two-level boson
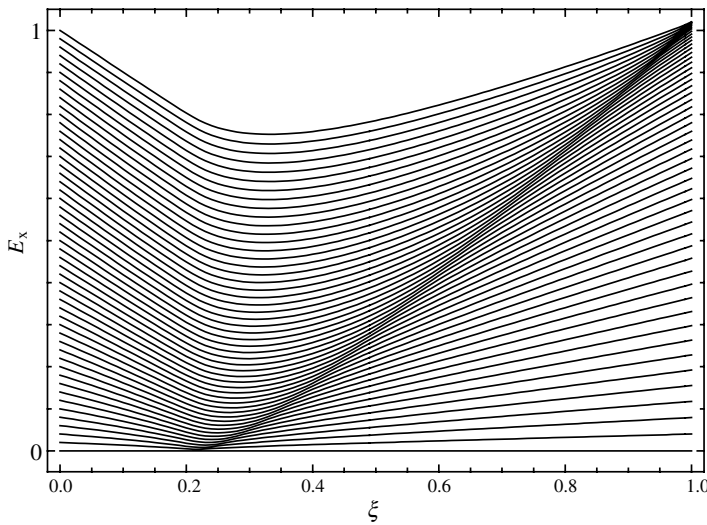
Fig. 1. Excitation energies for the two-level fermionic pairing model (2.7) with particle number $N = 100$, at half-filling and zero seniority, as a function of the control parameter ξ.

models and the two-level pairing model is established for arbitrary dimension in the appendices, where some further mathematical definitions and identities are also provided for reference.

2. Bosonic and fermionic two-level models

Ground state QPTs have been studied extensively (e.g., Refs. [2,15–17]) for the two-level boson models, or s–b models, defined in terms of a singlet boson $s^{(0)}$ and a $(2L + 1)$-fold degenerate boson $b^{(L)}$ (Fig. 2a). Models in this class include the U(6) interacting boson model (IBM) for nuclei ($L = 2$) [12], which is defined in terms of $s^{(0)}$ and $d^{(2)}$ bosons, and the U(4) vibron model for molecules ($L = 1$) [18]. Also, the Lipkin model [11] has several isomorphic realizations, defined variously in terms of systems of interacting fermions, interacting spins, or interacting bosons (Schwinger realization). This last realization falls into the two-level boson model categorization, as the $L = 0$ case. So far, excited state QPTs have been considered in the Lipkin model [5,6] and the IBM [7–9], both of which are examples of s–b two-level models.
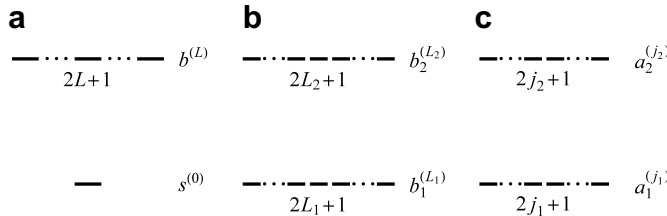

Fig. 2. Single-particle level degeneracies for the various classes of two-level models considered: (a) the s–b boson models, (b) the more general two-level bosonic pairing models, and (c) the two-level fermionic pairing models.

The s–b two-level models are described by the $U(n + 1)$ algebraic structure

$$U(n + 1) \supset \left\{ \begin{array}{c} SO(n + 1) \\ U(n) \end{array} \right\} \supset SO(n) \supset SO(3), \tag{2.1}$$

where $n = 2L + 1$. The $U(n + 1)$ generators are given in tensor form by $(s^\dagger \times \tilde{s})^{(0)}, (s^\dagger \times \tilde{b})^{(L)}, (b^\dagger \times \tilde{s})^{(L)}$, and $(b^\dagger \times \tilde{b})^{(\lambda)}$ (see Appendix A for detailed definitions). If the Hamiltonian is simply taken as the Casimir operator (A.11) of either of the subalgebras, $SO(n + 1)$ or $U(n)$, a dynamical symmetry is obtained. The $U(n)$ symmetry is geometrically related to the n-dimensional harmonic oscillator, the $SO(n + 1)$ symmetry to the n-dimensional rotator-vibrator (e.g., Ref. [19]).

The ground state QPT in the two-level boson models arises as the Hamiltonian is varied linearly between the two dynamical symmetries, for instance, by varying ξ in the Hamiltonian

$$\hat{H} = \frac{(1 - \xi)}{N} \hat{N}_b - \frac{\xi}{N^2} (s^\dagger \tilde{b} + b^\dagger \tilde{s}) \cdot (s^\dagger \tilde{b} + b^\dagger \tilde{s}), \tag{2.2}$$

where $\hat{N}_b \equiv (-)^L b^\dagger \cdot \tilde{b}$ is the b-boson occupancy, $\tilde{T}_\mu^{(\lambda)} \equiv (-)^{\lambda - \mu} T_{-\mu}^{(\lambda)}$, and $U^{(\lambda)} \cdot V^{(\lambda)} \equiv (-)^L (2L + 1)^{1/2} (A \times B)^{(0)}$. This Hamiltonian yields the $U(n)$ symmetry for $\xi = 0$ and the $SO(n + 1)$ symmetry for $\xi = 1$. The Hamiltonian is invariant under the common $SO(n)$ algebra in (2.1) and therefore conserves a $(2L + 1)$-dimensional angular momentum quantum number v. As ξ is increased from $\xi = 0$, the increasing strength of the interaction between s and b levels changes the structure of the ground state from a pure s-boson condensate to a condensate involving both types of bosons. For asymptotically large values of the total particle number $N \equiv N_s + N_b$, the change is abrupt. A second-order ground state QPT is well known to occur for $\xi_c = 1/5$, with all the properties enumerated in Section 1. [The coefficients in (2.2) are scaled by appropriate powers of N to guarantee that the location of the critical point is independent of N in the large-N limit.] With more complex interactions in the Hamiltonian, first-order QPTs, such as the physically important U(5)–SU(3) phase transition in the IBM, may also be obtained [2,15,20]. The conditions under which such first-order phase transitions occur in an arbitrary $U(n + 1)$ model are outlined in Ref. [21]. However, only second-order ground state QPTs will be considered here.

We observe, moreover, that the $U(n + 1)$ two-level boson models are special cases of an even larger family of models, the two-level pairing models with quasispin Hamiltonians. Two-level pairing models can be defined for systems of either bosons or fermions. The two-level pairing models undergo a second-order *ground state* QPT [22]. Therefore, it is natural to consider the possibility that *excited state* QPTs may occur within the context of this broader family of models as well.

The quasispin pairing Hamiltonian is of the form

$$\hat{H} = \sum_j \varepsilon_j \left(\sum_m c_{jm}^\dagger \tilde{c}_{jm} \right) + \frac{1}{4} \sum_{j'j} G_{j'j} \left(\sum_{m'} c_{j'm'}^\dagger \tilde{c}_{j'm'}^\dagger \right) \left(\sum_m \tilde{c}_{jm} c_{jm} \right), \tag{2.3}$$

where the summation indices j and j' run over the single-particle levels, and m and m' run over their substates. The c_j may represent either bosonic operators $b_1^{(L_1)}$ and $b_2^{(L_2)}$ (Fig. 2b) or fermionic operators operators $a_1^{(j_1)}$ and $a_2^{(j_2)}$ (Fig. 2c), as appropriate. Although the Hamiltonian (2.3) superficially appears quite different from the $U(n + 1)$ two-level boson

model Hamiltonian (2.2), the two are in fact equivalent [23,24]. The detailed relationship between the models is established for arbitrary n in Appendix A.

It is well known that the pairing Hamiltonian (2.3) can be expressed in terms of the generators $\hat{S}_{j+}, \hat{S}_{j-}$, and $\hat{S}_{jz}$ of a quasispin algebra (A.2), as

$$\hat{H} = \sum_j \varepsilon_j (2\hat{S}_{jz} \mp \Omega_j) + \sum_{j'j} G_{j'j} \hat{S}_{j'+} \hat{S}_{j-}, \tag{2.4}$$

where $\Omega_j \equiv (2j+1)/2$, and the upper and lower signs apply in the bosonic and fermionic cases, respectively. The algebra is either an SU(1,1) algebra if the operators are bosonic [25] or an SU(2) algebra if the operators are fermionic [26]. However, the pairing models are also characterized by an overlaid $U(n_1 + n_2)$ algebraic structure, described further in Ref. [27], either

$$U(n_1 + n_2) \supset \left\{ \begin{array}{c} SO(n_1 + n_2) \\ U_1(n_1) \otimes U_2(n_2) \end{array} \right\} \supset SO_1(n_1) \otimes SO_2(n_2) \supset SO_{12}(3) \tag{2.5}$$

in the bosonic case (with $n_1 = 2L_1 + 1$ and $n_2 = 2L_2 + 1$) or

$$U(n_1 + n_2) \supset \left\{ \begin{array}{c} Sp(n_1 + n_2) \\ U_1(n_1) \otimes U_2(n_2) \end{array} \right\} \supset Sp_1(n_1) \otimes Sp_2(n_2) \supset SU_{12}(2) \tag{2.6}$$

in the fermionic case (with $n_1 = 2j_1 + 1$ and $n_2 = 2j_2 + 1$), directly generalizing the $U(n+1)$ algebraic structure (2.1) of the s–b boson models. The $U(n_1 + n_2)$ generators are of the form $(c_1^\dagger \times \tilde{c}_1)^{(\lambda)}, (c_1^\dagger \times \tilde{c}_2)^{(\lambda)}, (c_2^\dagger \times \tilde{c}_1)^{(\lambda)}$, and $(c_2^\dagger \times \tilde{c}_2)^{(\lambda)}$. The $SO_1(n_1)$ and $SO_2(n_2)$ [or $Sp_1(n_1)$ and $Sp_2(n_2)$] algebras provide conserved n_1-dimensional and n_2-dimensional angular momentum quantum numbers (v_1 and v_2), which are equal to the seniority quantum numbers defined in the quasispin formulation.

The ground state QPT in the general two-level pairing models is between the $SO(n_1 + n_2)$ or $Sp(n_1 + n_2)$ dynamical symmetry and the $U_1(n_1) \otimes U_2(n_2)$ dynamical symmetry. To choose a transitional Hamiltonian for the general pairing models consistent with the Hamiltonian already used for the s–b boson models, we observe that the Hamiltonian (2.2) may be reexpressed (see Appendix A) in pairing form as

$$\hat{H} = \frac{(1-\xi)}{N} \hat{N}_2 + \frac{4\xi}{N^2} (-)^{L+1} (\hat{S}_{1+} \pm \hat{S}_{2+})(\hat{S}_{1-} \pm \hat{S}_{2-}) \tag{2.7}$$

to within an additive constant, where the full relation is given explicitly in (A.17). With this form of Hamiltonian for the pairing models, the ground state QPT again occurs at $\xi_c = 1/5$.

Since QPTs occur in the limit of large particle number, an important distinction arises between bosonic and fermionic models. Arbitrarily large particle number can be achieved in the *bosonic* models, even for fixed level degeneracies, simply by increasing the total occupancy. For a *fermionic* model, however, the total occupancy is limited by Pauli exclusion to the total degeneracy $[(2j_1 + 1) + (2j_2 + 1)]$. Therefore, the limit of large particle number can only be achieved if the number of available substates in each level is simultaneously increased. For two fermionic levels of equal degeneracy ($j_1 = j_2 \equiv j$), half-filling is achieved for $N = 2j + 1$.

It will be convenient to make extensive use of the U(3) two-dimensional vibron model [28–30] for illustration in this article. The U(3) vibron model is the simplest two-level model which still retains a nontrivial angular momentum or seniority quantum number (unlike the Lipkin model).
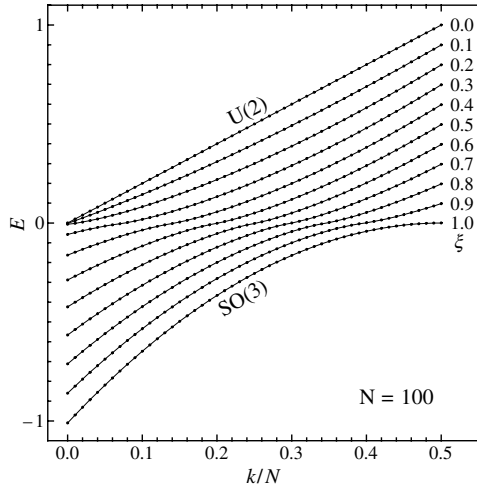
Fig. 3. Eigenvalue spectra for the U(3) vibron model $l = 0$ states ($N = 100$), for several specific values of the Hamiltonian parameter ξ. Eigenvalues are plotted with respect to the scaled excitation quantum number k/N.

First, note that single-particle levels in bosonic pairing models (Fig. 2a and b) are only restricted to odd degeneracies (i.e., $2L + 1$ with L integer) if a physical three-dimensional angular momentum subalgebra SO(3) is required in (2.1) or (2.5). The pairing interaction only requires the definition of time-reversed pairs. It therefore suffices to have an "M" quantum number, with pairs $\pm M$, without necessity for an "L" quantum number. The pairing interaction can therefore be defined for an even number of bosons, and the interaction within each level is described by SO(n) with n even.[1] Bosonic levels of even degeneracy arise naturally in problems lacking three-dimensional rotational invariance.

The U(3) vibron model may be obtained by considering the U(4) vibron model ($L = 1$) and eliminating the substate $b_0^{(1)}$. This leaves a U(3) algebraic structure, with SO(3) and U(2) dynamical symmetries. The geometrical coordinates associated with the U(4) model describe three-dimensional dipole motion (as in a linear dipole molecule). However, elimination of $b_0^{(1)}$ "freezes out" motion in the z direction, so the U(3) model instead describes two-dimensional motion in the xy plane. The U(2)–SO(3) transitional Hamiltonian, in Casimir form, is [28,29],

$$\hat{H} = \frac{(1 - \xi)}{N} \hat{N}_b - \frac{\xi}{N^2} \left[\frac{1}{2} \left(\hat{D}_+ \hat{D}_- + \hat{D}_- \hat{D}_+ \right) + \hat{l}^2 \right], \tag{2.8}$$

where $\hat{D}_\pm \equiv \pm \sqrt{2}(b_{\pm 1}^\dagger s_0 - s_0^\dagger b_{\mp 1})$. This is the two-dimensional equivalent of (2.2), to within an additive constant. The conserved two-dimensional angular momentum is $\hat{l} = b_{+1}^\dagger b_{+1} - b_{-1}^\dagger b_{-1}$. The eigenvalue spectra of $l = 0$ states, for various values of ξ, are shown in Fig. 3. The spectra for the U(2) dynamical symmetry ($\xi = 0$) and the SO(3)

---

[1] However, pairing is not well-defined for the converse situation, a fermionic level of odd degeneracy. With an odd number of substates, one ("$m = 0$") must necessarily be its own conjugate under time reversal. Creation of a time-reversed pair involving this substate is Pauli forbidden. The corresponding algebra, Sp(n) with n odd, is not defined.

dynamical symmetry ($\xi = 1$) have simple analytic forms [28]. Note also the spectrum for the ground state QPT ($\xi = 0.2$).

3. Semiclassical dynamics

3.1. Coordinate Hamiltonian

Each of the many-body models considered in Section 2 has an associated classical Hamiltonian, defined with respect to classical coordinates and momenta, which is obtained through the use of coherent states [2,31,32]. The basic properties of the excited state quantum phase transition follow from the semiclassical analysis of a double-well potential with a parabolic barrier (Fig. 4c) or, in higher dimensions, a sombrero potential (also known as the "champagne bottle" potential [33]). The semiclassical dynamics for these potentials has been studied in depth [33–37], and the connection with ESQPT phenomena in the Lipkin model and higher-dimensional s–b boson models has been made in Refs. [4,6,8,9]. In particular, at the energy of the top of the barrier, the classical action undergoes a logarithmic singularity, which leads semiclassically to the prediction of an infinite level density. Here we do not attempt a comprehensive recapitulation of the existing analysis but rather briefly summarize the essential points and derive some results specifically relevant to the observables of interest in phase transitional phenomena.
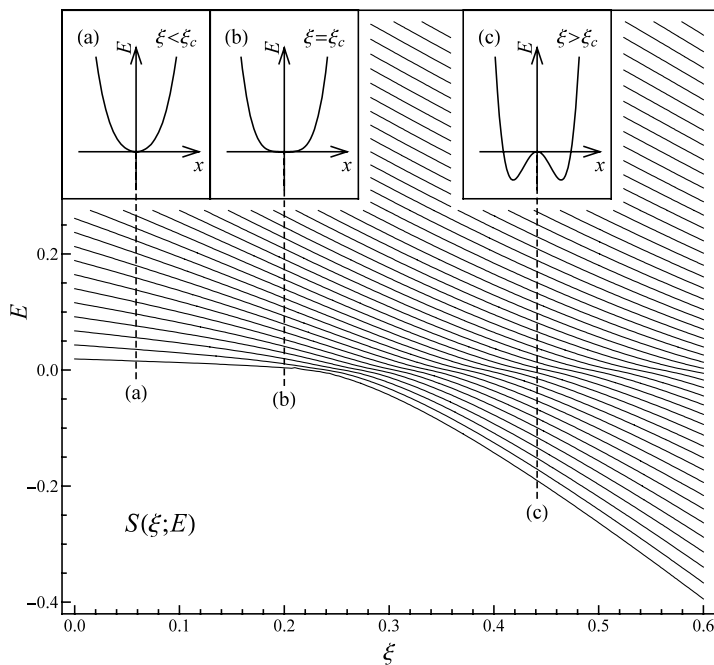

Fig. 4. Contour plot showing the global structure of the classical action $S(\xi; E)$ for the geometric Hamiltonian (3.1) or (3.2), through the different regimes determined by the shape of the quadratic-quartic potential energy function, which is shown for (a) $\xi < \xi_c$, (b) $\xi = \xi_c$, and (c) $\xi > \xi_c$. The individual contours are related semiclassically to the evolution of the level eigenvalues $E_k(\xi)$.

For the quasispin models of Section 2, the two superposed algebraic structures (quasispin and unitary) give rise to two alternative sets of coherent states and therefore to two realizations of the classical dynamics. The SU(1, 1) or SU(2) quasispin algebra yields a one-dimensional dynamics (the phase space is a Bloch sphere or hyperboloid [31, Ch. 6]) which is common to all the quasispin models. The dynamics arising from the quasispin algebra therefore highlights aspects universal to these models, yielding the basic double-well potential (Fig. 4c) and therefore indicating that all should exhibit an ESQPT at the energy of the top of the barrier. In contrast, the coherent states obtained from the unitary $U(n_1 + n_2)$ algebra yield a much richer classical dynamics, in $n_1 n_2$ dimensions, associated with the coset space $U(n_1 + n_2)/[U(n_1) \otimes U(n_2)]$ [31, Ch. 9]. This more complete dynamics, so far only fully investigated for the *s–b* models [38,39], yields a much more detailed description of the system. The dynamics obtained from the quasispin algebra is essentially a one-dimensional projection or "shadow" of the full dynamics arising from the unitary algebra, as described by Feng et al. [2] for the IBM. In particular, the presence of angular degrees of freedom and conserved angular momentum quantum numbers have significant consequences for the ESQPT [8,9].

First, let us summarize the classical Hamiltonian obtained from the $U(n + 1)$ coherent states for the *s–b* model. The classical Hamiltonian acts on n coordinates and their conjugate momenta. However, for the SO(n)-invariant interaction in (2.2), the Hamiltonian is invariant under rotations in the n-dimensional space and can therefore be expressed solely in terms of a radial coordinate r, its conjugate momentum p_r, and a conserved angular kinetic energy $T_\vartheta(v)$, as [9,17,39]

$$\hat{H} = \frac{1-\xi}{2N^2}[p_r^2 + r^{-2}T_\vartheta(v)] + \frac{\xi}{N^2}[r^2 p_r^2 + T_\vartheta(v)] + \frac{1-5\xi}{2}r^2 + \xi r^4, \tag{3.1}$$

where $T_\vartheta(v)$ has eigenvalue $v(v + n - 2)$ and the coordinate r is defined only on the domain $0 \leqslant r \leqslant \sqrt{2}$.[2] The eigenvalue problem for (3.1) therefore has the form of a *radial* Schrödinger equation with a quadratic-quartic potential, except for the appearance of the position-dependent kinetic energy term proportional to $r^2 p_r^2$. For the one-dimensional case, i.e., the Lipkin model, the centrifugal term is not present, and the coordinate and momentum are more aptly denoted by x and p, so

$$\hat{H} = \frac{1-\xi}{2N^2}p^2 + \frac{\xi}{N^2}x^2 p^2 + \frac{1-5\xi}{2}x^2 + \xi x^4, \tag{3.2}$$

where here both negative and positive values of the coordinate x are allowed $(-\sqrt{2} \leqslant x \leqslant +\sqrt{2})$.

The role of $\hbar^2/(2m)$ in the usual Schrödinger equation is taken on by the coefficient of p_r^2 or p^2 in (3.1) or (3.2). We therefore make the identification $\hbar \to N^{-1}$, with the coordinate-dependent mass $m(x) = (1 - \xi + 2\xi x^2)^{-1}$.

The forms assumed by the quadratic-quartic potential in (3.1) or (3.2), $V(x) = (1 - 5\xi)x^2/2 + \xi x^4$, are summarized for convenience in Fig. 4a–c. For the radial problem, of course, only the positive abscissa is relevant. For $\xi < 1/5$, the potential has a single minimum, at $x = 0$, which is locally quadratic. For $\xi = 1/5$, the critical value for the ground state QPT, the potential is pure quartic. For $\xi > 1/5$, the familiar dou-

---
[2] In obtaining (3.1) from Ref. [39], a scaling transformation $r \to N^{1/2}r$ has been made, and a constant term of order $1/N$ has been suppressed.

ble-well potential is obtained (or the sombrero potential for $n > 1$). For the Hamiltonian (3.1) or (3.2), the zero in energy is such that the top of the barrier is always at $E = 0$, independent of ξ.

3.2. Singular properties of the action

The main semiclassical features of levels at energies near the top of the barrier are obtained by noting that for $E = 0$ the classical velocity $v(E, x) = [2[E − V(x)]/m(x)]^{1/2}$ locally vanishes at the top of the barrier ($x = 0$). While indeed the classical velocity also vanishes at the ordinary linear turning points of a potential well, the vanishing slope at the top of the barrier presents a qualitatively broader "flat" region over which the classical velocity is small. Thus, the semiclassical motion has a long "dwell time" in the vicinity of $x = 0$. This leads to two essential results, namely (1) an infinite period $\tau = \oint v(E, x)^{-1} \mathrm{d}x$ for classical motion across the top of the barrier and (2) strong localization of the semiclassical probability density $P(x) \propto v(E, x)^{-1}$ at the top of the barrier [6].

The first-order semiclassical analysis provides a simple guidemap to the properties of the spectrum as a whole and also provides an explanation for the singularity in level density as the top of the barrier is approached. We consider the one-dimensional problem (3.2), but the results apply equally to the radial problem (3.1) with $v = 0$. For the Hamiltonian (3.2), the usual first-order WKB quantization condition [40] becomes

$$S(\xi; E) = \left(k + \frac{1}{2}\right) 2\pi N^{-1}, \tag{3.3}$$

with $k = 0, 1, \ldots$, where the action $S \equiv \oint p \, \mathrm{d}x$ over a full classical period of motion is given by the integral

$$S(\xi; E) = 2 \int_{x_1(E)}^{x_2(E)} \mathrm{d}x [2m(x)[E − V(x)]]^{1/2} \tag{3.4}$$

between classical turning points $x_1(E)$ and $x_2(E)$.[3] The action depends upon ξ variously through $m(x)$, $V(x)$, and the turning points.

The quantization condition (3.3) implicitly gives the adiabatic evolution of the energy $E_k(\xi)$ of a given level with respect to the parameter ξ. Since (3.3) enforces that $S(\xi; E)$ be constant if k is held fixed, the curve describing $E_k(\xi)$ is simply a contour of $S(\xi; E)$ in the ξ–E plane. These contours, calculated numerically for the Hamiltonian (3.2) [or (3.1) with $v = 0$] are plotted in Fig. 4. A compression of energy levels at $E = 0$ is visible qualitatively even here. [In Fig. 1, the $E_k(\xi)$ are plotted as *excitation* energies and therefore cannot be compared directly with Fig. 4. More appropriate plots for comparison may be found in the following section, e.g., Fig. 8a.] The derivative $\mathrm{d}E_k/\mathrm{d}\xi$ along a single contour of $S(\xi; E)$ is plotted in Fig. 5a. Note that $\mathrm{d}E_k/\mathrm{d}\xi$ undergoes a singularity in which $\mathrm{d}E_k/\mathrm{d}\xi \to 0$ but $\mathrm{d}^2 E_k/\mathrm{d}\xi^2 \to \pm\infty$, at a critical value $\xi = \xi_c^{\mathrm{ex}}$.

---

[3] Some bookkeeping issues naturally must be taken into account in the one-dimensional double-well problem (Fig. 4c). For $E < 0$, i.e., below the barrier, the two wells are classically isolated. Applying the quantization condition with S evaluated over one of the wells in isolation is equivalent to counting only states of one parity (symmetric or antisymmetric). For $E > 0$, applying the quantization condition with S evaluated over the full well counts states of both parity. Questions as to the proper transition between the regimes $E < 0$ and $E > 0$ are somewhat artificial, since the validity conditions for (3.3) break down at $E \approx 0$.
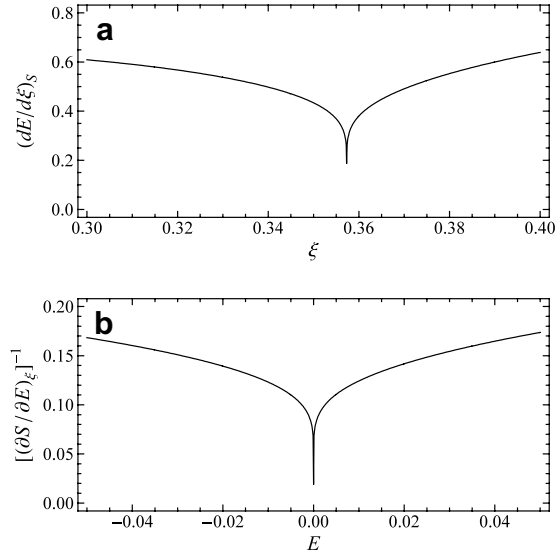
Fig. 5. Singularities in derivatives of the classical action (3.4) for the geometric Hamiltonian (3.1) or (3.2). (a) The derivative $dE/d\xi$ along a contour of $S(\xi; E)$ (Fig. 4), related semiclassically to the adiabatic evolution of the level energy. (b) The inverse of the partial derivative $(\partial S/\partial E)_\xi$, proportional to the semiclassical estimate for the gap.

In semiclassical analysis, the gap or level density is directly related to the classical period. From the quantization condition (3.3), it follows that the semiclassical estimate of the gap between adjacent levels ($\Delta = dE_k/dk$) is $\Delta(E) = 2\pi N^{-1}(\partial S/\partial E)^{-1}$. By differentiation of (3.4), the gap is simply $\Delta(E) = 2\pi N^{-1}\tau^{-1}$. As already noted for the ESQPT [6], the period τ becomes infinite at $E = 0$ and, equivalently, the gap $\Delta(E)$ vanishes. An explicit calculation of $(\partial S/\partial E)^{-1}$ as a function of E for the classical Hamiltonian (3.2) is shown in Fig. 5b. Note that $(\partial S/\partial E)^{-1}$ undergoes a singularity in which $(\partial S/\partial E)^{-1} \to 0$ but $(\partial^2 S/\partial E^2)^{-1} \to \pm\infty$, at the critical energy $E_c = 0$.

For nonzero angular momentum v, the origin ($r = 0$) is classically forbidden due to the centrifugal term in (3.1), which causes the wave function probability near the origin to be suppressed. This mitigates the effects just described, by masking the top of the barrier and precluding the long semiclassical dwell time at the origin [9]. The dependence of the Hamiltonian (3.1) on v is through the coefficient of the centrifugal term, which is proportional to $T_\vartheta(v)/N^2 \approx (v/N)^2$. Therefore, the phenomena associated with the ESQPT can be expected to be suppressed for sufficiently large v at any *given* value of N. On the other hand, the angular momentum effects at any *given* value of v are negligible for sufficiently large N. That is, the signatures of the ESQPT persist for small v ($v/N \ll 1$) and only disappear for v/N of order unity (as illustrated quantitatively in Section 4.1).

3.3. Asymptotic spectrum

Let us now consider more precisely the form of the singularity in the spectrum in the immediate neighborhood of the ESQPT. As the wave function becomes increasingly well-localized near the top of the barrier for $E \to 0$, it should become an increasingly good

approximation to treat the barrier as a pure inverted oscillator potential, $V(x) = -Ax^2$. The position-dependent kinetic energy term ($\propto x^2 p^2$) also becomes irrelevant.

In the action integral (3.4), the classical turning point at the barrier is $x_1(E) = (E/A)^{1/2}$ for $E < 0$, or for $E > 0$ integration simply extends to the origin. The distant turning point $x_2(E)$ is a slowly varying function of E which does not contribute to the singularity, so we may take it to be a constant. (In any case, for the actual potential, the approximation of a pure parabolic barrier breaks down well before the distant turning point is reached.) The action integral for $E > 0$ is therefore

$$\hbar^{-1} S(E) = \frac{2}{\hbar} \int_0^{x_2} dx [2m(E + Ax^2)]^{1/2},$$
$$= \frac{4}{\hbar\omega} E \int_0^{(A/E)^{1/2} x_2} du (1 + u^2)^{1/2}, \tag{3.5}$$

where for the inverted oscillator Hamiltonian $\hat{H} = [\hbar^2/(2m)]p^2 - Ax^2$, we have defined $\hbar\omega = 2[\hbar^2/(2m)]^{1/2} A^{1/2}$ by analogy with the conventional harmonic oscillator.

Expanding this action integral [41, (2.271.3)] for $E \approx 0$ yields

$$\hbar^{-1} S(E) = \frac{1}{\hbar\omega} (-E \log E + \alpha_0 + \alpha E + \cdots), \tag{3.6}$$

where α_0 and α are constants, i.e., depend only on the potential parameters A and x_2. An essentially identical result is obtained for $E < 0$, with the replacement $E \to |E|$ [41, (1.646.2)]. The singular behavior for energies near the top of the barrier therefore arises from the $E \log E$ term.[4] The quantization condition (3.3) takes on the form

$$-E \log E + \alpha E + \cdots = 2\pi\hbar\omega(k - k_c), \tag{3.7}$$

where $E = 0$ is obtained for $k = k_c$. If the energy dependence in (3.7) is truncated at the terms shown, i.e., linear order in E, this quantization condition can be solved for $E(k)$ in terms of the Lambert W function, by (B.5), yielding $E(k) = -2\pi\hbar\omega(k - k_c)/W[-e^{-\alpha}2\pi\hbar\omega(k - k_c)]$. The relevant properties of the W function are summarized in Appendix B.

For the Hamiltonian (3.2), the top of the barrier is described by an oscillator constant which may be read off from the coefficients of the p^2 and x^2, giving

$$\hbar\omega = \frac{\Xi(\xi)^{1/2}}{N}, \tag{3.8}$$

where

$$\Xi(\xi) \equiv (1 - \xi)(1 - 5\xi). \tag{3.9}$$

The oscillator constant thus depends upon both ξ and N. The same function $\Xi(\xi)$, interestingly, also enters into the *ground state* QPT scaling properties, as obtained by the continuous unitary transform method in Ref. [44]. The semiclassical estimate for the eigenvalue spectrum in the vicinity of the ESQPT is therefore

---

[4] Since the Schrödinger equation for a pure parabolic barrier is exactly solvable in terms of parabolic cylinder functions [42], the $|E|\log|E|$ dependence can also be obtained by explicitly matching this solution for the wave function in the vicinity of the barrier to asymptotic WKB wave functions away from the barrier [43].

$$E(N, \xi, k) = -\frac{2\pi\Xi(\xi)^{1/2}(k - k_c)/N}{W[-\mathrm{e}^{-\alpha}2\pi\Xi(\xi)^{1/2}(k - k_c)/N]}, \tag{3.10}$$

where α will contain a dependence on ξ as well. Differentiation with respect to k, making use of (B.4), yields a semiclassical estimate

$$\Delta(N, \xi, k) = -\frac{2\pi\Xi(\xi)^{1/2}/N}{W[-\mathrm{e}^{-\alpha}2\pi\Xi(\xi)^{1/2}(k - k_c)/N] + 1} \tag{3.11}$$

for the energy gap between adjacent excited states.

Since the excitation quantum number and particle number enter into the quantization condition (3.3) together in the combination k/N, the spectrum and finite-size scaling properties are inextricably linked at the semiclassical level.[5] The expression (3.11), considered as a function of N at fixed k, provides an estimate for the scaling of the gap at the $(k - k_c)$th eigenvalue above or below $E = 0$. The large-N behavior follows from the known asymptotic form (B.2) of the W function as a sum of logarithms for $x \to 0^-$ (see Fig. B.1). The values of x relevant to (3.11) in the vicinity of the ESQPT are of the order $x \sim -N^{-1}$. The asymptotic form (B.2) provides a good approximation to $W(x)$ for reasonable N, e.g., accurate to 1% by $N \sim 10^5$.

For very large N, the scaling behavior is in principle even simpler. The $\log(-x)$ term in (B.2) outgrows the $\log[-\log(-x)]$ term as $x \to 0^-$. With this logarithmic approximation, an extreme asymptotic estimate

$$N\Delta \sim -\frac{2\pi\Xi(\xi)^{1/2}}{\log(k - k_c) - \log N + \log[2\pi\Xi(\xi)^{1/2}] - \alpha + 1} \sim \frac{2\pi\Xi(\xi)^{1/2}}{\log N} \tag{3.12}$$

is obtained, recovering the logarithmic scaling noted by Leyvraz and Heiss [6]. However, even for $N \sim 10^{10}$, the approximation $W(x) \sim \log(-x)$ yields an error of >10% and therefore is of limited *quantitative* value for systems of typical "mesoscopic" size.

Note that the quantization condition as given in (3.3) is derived under the assumption that the classical turning points are *well-separated* (by several de Broglie wavelengths) and that the potential is locally *linear* at these turning points [40]. This suffices for the analysis of levels which are not close in energy to the top of the barrier. However, for $E \approx 0$, the barrier presents a *quadratic* classical turning point. (Equivalently, the linear turning points on either side of the barrier approach each other, violating the assumption of sufficient separation.) For accurate quantitative analysis of the levels immediately surrounding $E = 0$, the more general phase-integral method must be applied [45]. For a smooth, symmetric double-well potential, the phase-integral method yields an approximate quantization condition [45, (3.47.1)]

$$\hbar^{-1}S(E) = 2\pi\left(k + \frac{1}{2}\right) - \tilde{\phi} + 2\beta_0'' \pm \arctan\exp(-K), \tag{3.13}$$

with k an integer, where the various phases appearing on the right hand side are defined in Ref. [45]. The full derivation involves the evaluation of contour integrals on the complex

---

[5] For the *ground state* QPT, the semiclassical potential is quartic (Fig. 4b). A simple application of the WKB formula gives a dependence $E(k/N) \sim (k/N)^{4/3}$, which simultaneously yields both the spectrum $E_k \sim k^{4/3}$ [Fig. 3 ($\xi = 0.2$)] and the scaling $\Delta \sim N^{-4/3}$ (Section 4.2).

extension of the coordinate axis and the consideration of complex-valued turning points for energies just above the barrier [45]. Quantitative solution of the problem is considered in detail in Refs. [35,37,46,47]. The effects of these corrections (3.13) relative to (3.3) are explored in Ref. [33]. The corrections are essential to the treatment of the first few eigenvalues above or below the barrier. However, here we are instead interested in extracting the basic nature of the singularity from the dependence of $S(E)$ on E in the vicinity of $E = 0$, for which the simple quantization condition (3.3) suffices.

4. Quantum properties

4.1. Eigenvalue spectrum

In a ground state QPT, the singular behavior of the system is simultaneously reflected in the eigenvalue spectrum (ground state energy and gap) and in the order parameters. From the preceding semiclassical analysis (Section 3), it is to be expected that a similar variety of interconnected phenomena occur at the ESQPT, and this is indeed borne out by the quantum calculations. Of course, the analogy between ground state QPT and ESQPT is far from exact, so let us now examine the results for spectra and order parameters obtained numerically from the full quantum calculation, to elucidate both the analogy with the ground state QPT and the applicability of the semiclassical results of Section 3.

While the ground state QPT may only be traversed by varying a Hamiltonian parameter, the locus of the ESQPT is a curve in the two-parameter space defined by the Hamiltonian parameter ξ and the excitation energy (as along the dense band in Fig. 1). Therefore, the ESQPT may be crossed either "horizontally", by varying ξ, or "vertically", by varying the excitation quantum number k (or, equivalently, the energy E) of the level being examined.

The energy spectrum consists of the set of eigenvalues $E_{N,\xi,k,\Lambda}$, which contain dependences on several quantities: the system size N, the Hamiltonian parameter ξ, the excitation quantum number k, and other conserved quantum numbers Λ (angular momenta or seniorities in the present models). For large N, however, k/N and Λ/N become essentially continuous variables. In the preceding section, it was seen that semiclassically the energy depends upon the quantum numbers only through these combinations k/N and Λ/N. We are therefore largely interested in the properties of the spectrum given by the function $E(\xi, k/N, \Lambda/N)$ of three quasi-continuous variables [17]. The dependence of the spectrum on *interaction*, *excitation quantum number*, and *angular momentum* is contained in the dependence of $E(\xi, k/N, \Lambda/N)$ on its three arguments.[6] Furthermore, note that the dependence on the argument k/N implicitly contains information not only on the excitation spectrum [when the function is considered as $E(k)$ at fixed N] but also on the *finite-size scaling behavior* [when the function is considered as $E(1/N)$ at fixed k]. The properties of $E(\xi, k/N, \Lambda/N)$ in the vicinity of the ground state, that is, for $k/N \ll 1$, have been studied in detail, at least for the s–b models. Here, instead, we are considering the regime $k/N \sim 1$.

---

[6] In the Hamiltonians (2.2) and (2.7), the coefficients of the one-body operators are scaled by N and the coefficients of the two-body operators are scaled by N^2. Often a Hamiltonian normalization differing by an overall factor of N is instead used, e.g., $\hat{H} = (1 - \xi)\hat{N}_b - (\xi/N)(s^\dagger\tilde{b} + b^\dagger\tilde{s}) \cdot (s^\dagger\tilde{b} + b^\dagger\tilde{s})$ for the s–b model. For the normalization (2.2) or (2.7), $E_{N,\xi,k,\Lambda}$ does indeed approach a limiting value $E(\xi, k/N, \Lambda/N)$ as $N \to \infty$, by (3.3). However, for the alternate normalization it is actually $N^{-1}E_{N,\xi,k,\Lambda}$ which approaches a limiting value as $N \to \infty$.

First, let us establish the common ground between the various models under consideration (Section 2), by a simple comparison of the energy spectra. Calculations are shown in Fig. 6 for the Lipkin model (Fig. 6a), the U(3) vibron model (Fig. 6b), a bosonic pairing model with equal degeneracies for both levels ($L_1 = L_2 = 1$) (Fig. 6c), and a fermionic pairing model with equal degeneracies ($j_1 = j_2 = 9/2$) (Fig. 6d). The calculations are all for a fixed, modest particle number ($N = 10$), so that individual eigenvalues are clearly distinguishable. In the comparison, we must distinguish the invariant subspaces of states for each model. Each eigenstate of the Lipkin model contains only even-N_b or odd-N_b components and is thus characterized by a grading quantum number g with values 0 and 1 ($g \cong N_b$ mod 2) or, equivalently, the parity $\pi = (-)^g$. The vibron model states are characterized by the angular momentum $l = 0, \pm 1, \ldots, \pm N$. The bosonic and fermionic pairing model states are characterized by seniority quantum numbers for each single-particle level, namely, v_1 and v_2.

Note the essentially identical evolution, with respect to ξ, of the even-parity ($g = 0$) states of the Lipkin model, the zero angular momentum ($l = 0$) states of the vibron model, and the zero seniority [$(v_1 v_2) = (00)$] states of both the bosonic and fermionic pairing models (solid curves in Fig. 6). The ground state energy is near constant, with $E_0 \approx 0$, for $\xi < \xi_c$ and decreases to $\lesssim -1$ for $\xi = 1$. The highest eigenvalue decreases approximately linearly
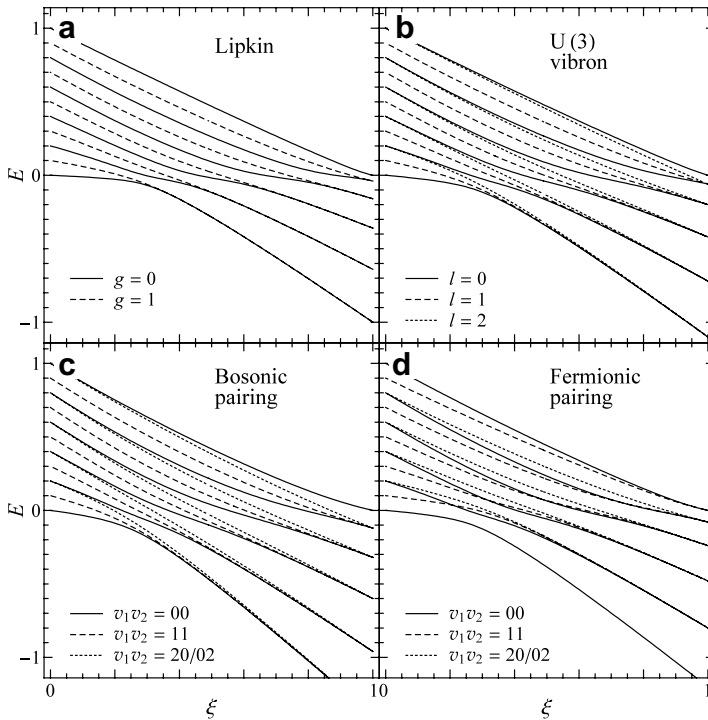

Fig. 6. Eigenvalues for (a) the Lipkin model (Schwinger realization), (b) the U(3) vibron model, (c) the bosonic pairing model ($L_1 = L_2 = 1$), and (d) the fermionic pairing model ($j_1 = j_2 = 9/2$), as functions of the coupling parameter ξ, all for total particle number $N = 10$. For the Lipkin model, both even-parity (solid curves) and odd-parity (dashed curves) levels are shown. For the other models, only the lowest angular momenta or seniorities are shown. A diagonal contribution $\xi(N + 2L_1 + 2L_2)/N$ has been subtracted from the Hamiltonian (2.7) for the bosonic pairing model [27].

with ξ, from 1 to 0. Various qualitative features associated with the ESQPT occur at $E \approx 0$ for $\xi > \xi_c$ for these models. Note especially the inflection points for these levels (solid curves) as well as the change in the pattern of degeneracies between different seniorities (or parities or angular momenta) at $E \approx 0$.

The major differences among the models lie in the degeneracy patterns at nonzero seniority, which depend upon the specific algebraic properties of the individual models [27]. At present, we will limit consideration of angular momentum effects to the *s–b* models, since for these only one angular momentum quantum number is involved, and *l* in the U(3) vibron model (Section 2) serves as a natural example for illustration.

The semiclassical analysis of Section 3 provided a simple set of predictions (Fig. 5) for the singular behavior of $E(\xi, k/N, \Lambda/N)$ as the ESQPT is crossed both "horizontally" [$E(\xi)$] and "vertically" [$E(k/N)$]. Namely, $E(\xi)$ undergoes a singularity in which the *slope* sharply approaches zero ($\partial E/\partial \xi \to 0$) (Fig. 5a) but with a *curvature* which becomes infinite and reverses sign ($\partial^2 E/\partial \xi^2 \to \pm \infty$), yielding a special divergent form of inflection point, as $\xi \to \xi_c^{ex}$. A similar singularity is expected in $E(k/N)$ (Fig. 5b) at the critical energy.

The actual diagonalization results at finite N show clear precursors of this form of singularity in E as ξ is varied. Even for the small system size ($N = 10$) considered in Fig. 6, each eigenvalue $E(\xi)$ undergoes an inflection [Fig. 6 (solid curves)] at an energy close to the expected critical energy, i.e., $E_c = 0$ for the Hamiltonians used. The derivative $\partial E/\partial \xi$ is shown for larger boson number ($N = 100$ and 1000) in Fig. 7a, for the U(3) vibron model
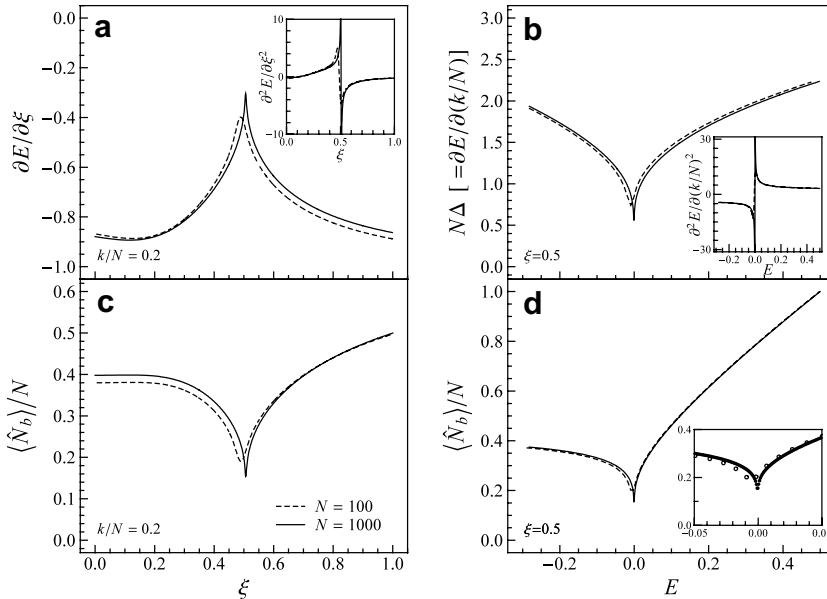

Fig. 7. Evolution of excited level energies and the order parameter $\langle \hat{N}_b \rangle$ across the ESQPT, as traversed both by varying ξ (left) and by varying E (right), i.e., "horizontally" and "vertically". Calculations are shown for the U(3) vibron model $l = 0$ states, with $N = 100$ (dashed curves) and 1000 (solid curves). (a) The derivatives $\partial E/\partial \xi$ and $\partial^2 E/\partial \xi^2$ (inset), for a specific excited level ($k/N = 0.2$). (b) The derivative $\partial E/\partial(k/N)$ or, equivalently, the scaled gap $N\Delta$, and $\partial^2 E/\partial(k/N)^2$ (inset), for $\xi = 0.5$. (c) The order parameter $\langle \hat{N}_b \rangle$ (rescaled by N) as a function of ξ for the same level as in (a). (d) The order parameter $\langle \hat{N}_b \rangle$ (rescaled by N) as a function of excitation energy, for the same ξ value as in (b). The discrete eigenstates are resolved at the expanded scale shown in the inset.

$l = 0$ states. The second derivative $\partial^2 E/\partial\xi^2$ is also shown (inset). The expected dip $\partial E/\partial\xi \to 0$ and divergent inflection $\partial^2 E/\partial\xi^2 \to \pm\infty$ both are present and become gradually sharper with increasing N.

For nonzero l in Fig. 6b, the inflection points in the eigenvalues as functions of ξ are washed out, as expected from the semiclassical analysis (for $l > 0$ the centrifugal term suppresses the probability density near $r = 0$, mitigating the effect of the barrier). For $N = 10$, the inflection points disappear even for the very lowest nonzero l values (dashed curves in Fig. 6b). Also for $N = 10$, the inflection points are suppressed for the negative parity ($g = 1$) states of the Lipkin model in Fig. 6a. Here a similar mechanism applies: negative parity states possess a node at $x = 0$, and the effect of the parabolic barrier at $x = 0$ is therefore again reduced. (To this extent, the grade in the Lipkin model is a surrogate for the angular momentum in the higher-dimensional boson models. The formal relation is given in Appendix A.) Compare also the curves for nonzero seniorities in Fig. 6c and d. While the change in behavior of the eigenvalues between $l = 0$ and nonzero l seems to be rather abrupt for the $N = 10$ illustration, it must be borne in mind that the relevant parameter for the semiclassical description was noted to be l/N, which can only be varied very coarsely when $N = 10$. The more gradual evolution of the ESQPT with l/N, as obtained for larger N, is considered further below.

The properties of the spectrum as the ESQPT is traversed "vertically" by varying the excitation quantum number for a single fixed Hamiltonian parameter value ξ are explored in Fig. 7b, again for the U(3) vibron model with $N = 100$ and 1000, now at the specific parameter value $\xi = 0.5$. The singularity in $E(\xi, k/N, \Lambda/N)$ with respect to k/N gives rise to the original, defining property of the ESQPT, namely the vanishing gap or infinite level density. The gap is simply the change in energy for a unit change in k quantum number, so in the limit where k/N is taken as a quasi-continuous variable we have $\partial E(\xi, k/N, \Lambda/N)/\partial(k/N) = N\Delta(\xi, k/N, \Lambda/N)$. The gap is shown as a function of energy, rather than of k, in Fig. 7b, so that the energy in the spectrum at which the precursors of the singularity occurs can be compared with the expected critical energy $E_c = 0$. The second derivative $\partial^2 E/\partial(k/N)^2$ is also shown (inset). The qualitative features $\partial E/\partial(k/N) \to 0$ and $\partial^2 E/\partial(k/N)^2 \to \pm\infty$ expected from the semiclassical analysis are indeed realized, more sharply with increasing N.

The inflection point of E with respect to k at $E = 0$ (though not its singular nature) is also immediately visible simply by inspection of the $l = 0$ spectra obtained for various ξ (Fig. 3). The spectra are concave downward with respect to k below $E = 0$ and concave upward above this energy. At the SO(3) limit, the entire spectrum falls below $E = 0$ and constant downward concavity follows from the exact formula [28] for the eigenvalues, quadratic in k. Although, here we are considering the dip in $\partial E/\partial k$ as a property of the ESQPT in a many-body interacting boson model, it should be noted that the dip arising for the associated two-dimensional Schrödinger equation is well known as the "Dixon dip" [48], with applications to molecular spectroscopy (see also Ref. [30]).

For nonzero l, as noted above, the relevant parameter governing the disappearance of the ESQPT is expected to be l/N. The eigenvalue spectrum for the U(3) vibron model with $N = 100$ indeed shows compression of the level density at the critical energy for $l = 0$ (Fig. 8a) and, conversely, no apparent compression of level density for large l/N (Fig. 8b), where $l = 25$ or $l/N = 1/4$ is shown in this example. (See Ref. [7] for analogous plots for the IBM.) However, the gradual nature of the evolution with l/N is seen by considering the dip in $\partial E/\partial k$, which becomes continuously less deep and less sharp as l/N is increased (Fig. 8c).
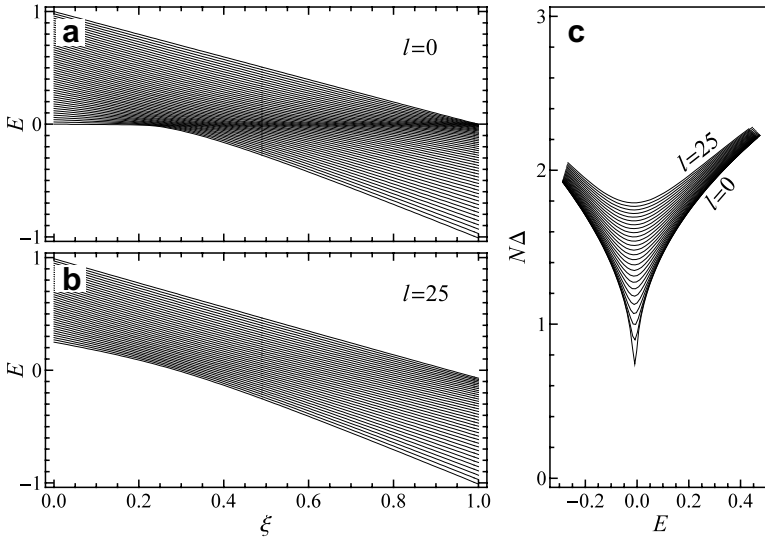
Fig. 8. Angular momentum dependence of spectral properties for the U(3) vibron model ($N = 100$). (a and b) Evolution of eigenvalues with ξ for $l = 0$ and $l = 25$, i.e., $l/N = 1/4$. (c) Dependence of the gap on excitation energy, as in Fig. 7b, for various l ($0 \leqslant l \leqslant 25$).

4.2. Finite-size scaling

The spectroscopic hallmark of the critical point of a QPT is not a *vanishing* gap *per se*, since the gap never strictly vanishes for finite system size, but rather the *nature* of its approach to zero as N increases. It is therefore essential to characterize the finite-size scaling behavior of the gap in the vicinity of the ESQPT. With the Hamiltonian normalization of (2.2), the gap Δ everywhere approaches zero with increasing N, so we are actually, more precisely, interested in the scaling of the gap at the ESQPT *relative* to the scaling elsewhere in the spectrum. For states well-separated from both the ground state QPT and ESQPT, the scaling is as $\Delta \sim N^{-1}$. For states in the vicinity of the *ground state* QPT, the gap vanishes more quickly than N^{-1}, as the power law $\Delta \sim N^{-4/3}$. This has been established both numerically and analytically for the various models under consideration [30,44,49–52].[7] The gap at the *excited state* QPT also approaches zero more rapidly than $\Delta \sim N^{-1}$. This is apparent even from the simple plot Fig. 7b, where $N\Delta$ is essentially independent of N away from the critical energy (compare the curves for $N = 100$ and $N = 1000$) but approaches zero with increasing N at the critical energy.

Let us now examine finite-size scaling more carefully, in particular, to see the extent to which the semiclassical expression (3.11) reproduces the scaling behavior. It is not *a priori* obvious that the semiclassical result (3.11) should yield the proper scaling properties for the eigenvalues in the vicinity of the ESQPT. Even in the solution of the ordinary Schrö-

---

[7] As noted above, different normalization conventions may be encountered for the model Hamiltonians. Overall multiplication of the Hamiltonian by a factor N gives rise to a superficial difference of unity in the finite-size scaling exponents.

dinger equation, the semiclassical analysis becomes unreliable for the first few eigenvalues in the vicinity of the top of the barrier [33–35].

First, in Fig. 9a, the actual form of the spectrum in the vicinity of the ESQPT, obtained by numerical diagonalization, is compared with the semiclassical estimate (3.10). Eigenvalues are shown for $N = 100$ and $N = 1000$. Note that k_c is simply determined as the value of k for which the energy eigenvalues cross zero. This must be interpolated between discrete eigenvalues, so k_c is in general noninteger. The singular logarithmic term in (3.6) has a coefficient which is predicted unambiguously from the value of $\hbar\omega$ (3.8) for the inverted oscillator, but no attempt is made here to directly calculate the coefficient α of the nonsingular linear term. Rather, α is simply chosen to numerically reproduce the linear trend in the eigenvalues in the vicinity of the ESQPT. The α value obtained from a limited number of eigenvalues around $E = 0$ therefore depends somewhat on both N and the number of eigenvalues considered. The gap, that is, the first difference of the eigenvalues in Fig. 9a, is plotted in Fig. 9b, together with the semiclassical estimate (3.11). The form of the singularity is well matched by the semiclassical estimate. (The parameter α essentially determines the normalization of the curve $\Delta[(k - k_c)/N]$.) The most significant deviation occurs for the first few eigenvalues around $E = 0$.

Some care must be taken in establishing exactly what gap is to be considered in the context of finite-size scaling, since the gap is a function of $k - k_c$, that is, how far above or below the ESQPT the gap is measured. The phase transition does not fall exactly "on" an eigenvalue (k_c is in general noninteger), the gap is varying singularly with k at k_c,
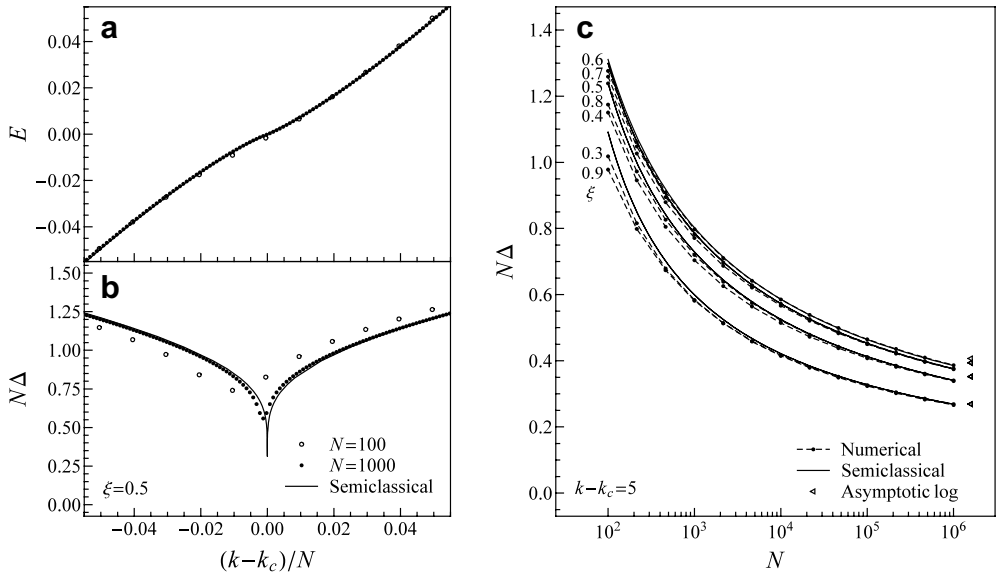

Fig. 9. Quantitative comparison of quantum and semiclassical results for the gap, including finite-size scaling properties, in the vicinity of the ESQPT ($E \approx 0$). Calculations are for the U(3) vibron model $l = 0$ states with $\xi = 0.5$. (a and b) Eigenvalue spectrum and its first difference, i.e., the gap, shown as functions of $(k - k_c)/N$ for $N = 100$ (open circles) and 1000 (solid circles). The semiclassical result (3.10) or (3.11) in terms of the W function (with $\alpha = 2.49$) is shown for comparison (solid curve). (c) Scaling of the gap with respect to N, evaluated at fixed quantum number $k - k_c = 5$ relative to the ESQPT, for $\xi = 0.3, 0.4,\dots,0.9$. The semiclassical results for the scaling (with $\alpha = 1.24, 1.92, 2.24$, and 2.35) are shown for comparison (solid curve). The results of the asymptotic logarithmic expression (3.12), evaluated at $N = 10^6$, are also indicated (open triangles).

and the quantum corrections are fluctuating most strongly for the first few eigenvalues in the vicinity of k_c [33]. Therefore, in considering the finite-size scaling at the mean-field level, it is only meaningful to examine the gap some sufficient number of eigenvalues above or below the ESQPT, but nonetheless close enough ($|k - k_c| \ll N$) that the scaling appropriate to the ESQPT dominates over the usual $\Delta \sim N^{-1}$ scaling.

The gap for $k - k_c = 5$ is plotted as a function of N, for $10^2 \leqslant N \leqslant 10^6$, in Fig. 9c. (The quantity plotted is essentially the gap between the fifth and sixth eigenvalues above $E = 0$, but interpolation is necessary, since $k - k_c$ is discrete and noninteger in the actual spectra.) Note foremost that the gaps for $\xi = 0.3$ and $\xi = 0.9$, or for $\xi = 0.4$ and $\xi = 0.8$, or for $\xi = 0.5$ and $\xi = 0.7$, converge towards each other for large N. Since $\Xi(\xi)$ is symmetric about $\xi = 0.6$ [see (3.9)], this demonstrates that the asymptotic behavior depends on ξ through $\Xi(\xi)$, as expected if the properties of the ESQPT are dominated by the $\hbar\omega$ value (3.8) of the parabolic top of the barrier. The semiclassical estimate (3.11) is shown for comparison (using only one fixed α value for each symmetric pair of ξ values, for simplicity) and appears to reasonably reproduce the finite-size scaling. The results of the simple logarithmic approximation $N\Delta \approx 2\pi\Xi(\xi)^{1/2}/N$ from (3.12), evaluated at $N = 10^6$, are also shown for reference.

4.3. Order parameters

Let us now consider the singularity in the order parameter $\langle \hat{N}_b \rangle$ (or $\langle \hat{N}_2 \rangle$), which plays a defining role for the ground state QPT. The evolution of the order parameter $\langle \hat{N}_b \rangle_k$ is shown as a function of ξ in Fig. 7c, again for the U(3) vibron model, for the same level ($k/N = 0.2$) considered in Fig. 7a. This quantity is closely related to the energy plotted in Fig. 7a, since

$$\frac{dE_k(\xi)}{d\xi} = \frac{1}{\xi}\left[E_k(\xi) - \frac{\langle \hat{N}_b \rangle_k}{N}\right] \tag{4.1}$$

by the Feynman–Hellmann theorem.

It is seen that $\langle \hat{N}_b \rangle_k$ undergoes a dip towards zero at $\xi = \xi_c^{ex}$, which becomes sharper and deeper with increasing N. At the semiclassical level, one of the essential characteristics of the ESQPT was localization of the wave function at $x = 0$, together with vanishing classical velocity (hence, $p^2 = 0$). In coordinate form, $\hat{N}_b \propto p^2/N^2 + x^2$ [with the coordinate definitions used in (3.2)], so the natural extension to the fully quantum description is localization of probability with respect to occupation number at $N_b \approx 0$. The order parameter is shown as a function of energy in Fig. 7d, for the same fixed ξ value ($\xi = 0.5$) considered in Fig. 7b. The "evolution" of properties with respect to excitation energy is of necessity discrete, since for finite N the eigenvalue spectrum is itself discrete (Fig. 7d inset). It is apparent from Fig. 7c and d that, while $\langle \hat{N}_b \rangle_k$ drops *towards* zero at the ESQPT, and the dip becomes sharper and deeper with increasing N, $\langle \hat{N}_b \rangle_k$ is far from actually reaching zero at the finite N being considered.

5. Quantum phases

So far we have considered the excited state quantum phase transition as a *singularity* in the *evolution* of the excited state properties rather than as a *boundary* between *phases*. A

central question which arises in connection with the ESQPT phenomenology concerns the meaning of "phases" for excited states, namely, whether or not the excited states on each side of the phase transition can meaningfully be considered to belong to qualitatively distinct phases. Of course, in thermodynamics, it is well known that *phase transitions*, in the sense of singularities, do not necessarily imply the existence of distinguishable *phases*, the liquid–vapor transition in the vicinity of a critical point being a classic counterexample. Here we approach identification of phases both through indirect measures of the structural properties of the states on either side of the ESQPT (e.g., order parameters and spectroscopic signatures) and directly through inspection of the wave functions.

For the ground state, the "phase" is simply indicated by the value of the order parameter $\langle \hat{N}_b \rangle_0$ (or $\langle \hat{N}_2 \rangle_0$). In the large-$N$ limit, the value of $\langle \hat{N}_b \rangle_0$ is qualitatively different on either side of ξ_c, namely, vanishing for $\xi < \xi_c$ and nonzero (growing towards $N/2$) for $\xi > \xi_c$. In contrast, for the excited states, $\langle \hat{N}_b \rangle_k$ does not show such a qualitative difference between the two sides of the ESQPT. Rather, $\langle \hat{N}_b \rangle_k \to 0$ as the level k crosses the ESQPT but is nonzero on *either* side (Section 4.3). Therefore, the expectation value $\langle \hat{N}_b \rangle_k$ by itself does not distinguish two "phases" for the excited states.

The reason is fundamentally related to the classical limit of the problem (Section 3). Recall that $\hat{N}_b \propto p^2/N^2 + x^2$. For the classical ground state, the kinetic energy vanishes, and the static equilibrium value for x is simply determined by the location of the minimum in the potential (2). For excited states, such a *static* quantity no longer provides a suitable measure of the phase at the classical level, since excited states (with nonzero kinetic energy) are not described by a single equilibrium position. Instead, one must consider a *dynamical* definition of phase, taking into account the topology of the classical orbits in the phase space [8,9]. The classical analogue of the "expectation value" of an observable is its time average over the classical motion, $\langle f(x,p) \rangle \equiv \tau^{-1} \oint f(x,p)v(E,x)^{-1}\,\mathrm{d}x$. This is also the semiclassical average with respect to the first-order WKB probability density $P(x) \propto v(E,x)^{-1}$, so the time average carries over naturally to the quantum expectation value. At the quantum level, the consequence of the breakdown of the static definition is that the expectation value $\langle \hat{N}_b \rangle_k$ does not provide an unambiguous measure of the phase of an excited state.

Nonetheless, there are qualitative changes in the spectrum across the ESQPT. In particular, the degeneracy patterns with respect to the angular momentum (or seniority) quantum number change from those characteristic of the $U(n_1) \otimes U(n_2)$ dynamical symmetry above the critical energy to those characteristic of the $SO(n_1 + n_2)$ dynamical symmetry below the critical energy. At the critical energy, a rapid rearrangement of degeneracies occurs. This is clearly visible for all the models in Fig. 6. The evolution of the eigenvalues for the U(3) model is shown in detail in Fig. 10, for more angular momentum values ($l \leqslant 5$) and for a larger particle number ($N = 25$) than in Fig. 6b. Note that the like-parity states (l odd or l even) form approximate degenerate multiplets [U(2)-like] above $E = 0$ for all ξ, while multiplets are composed of all l values [SO(3)-like] below this energy. For the Lipkin model, the transition between degeneracy patterns is understood from the geometric Hamiltonian, as noted in Ref. [4], in terms of degenerate parity doublets below the barrier and lifting of this degeneracy above the barrier. For the higher-dimensional models, the change in degeneracies at the ESQPT is indicative of the breakdown of the adiabatic separation of rotational and radial vibration degrees of freedom at the critical energy.

For the ground state QPT, the persistence of the degeneracies associated with the symmetry limits as the QPT is approached, in spite of strong symmetry-breaking interactions, has been explained in terms of quasidynamical symmetry [53]. The qualitative
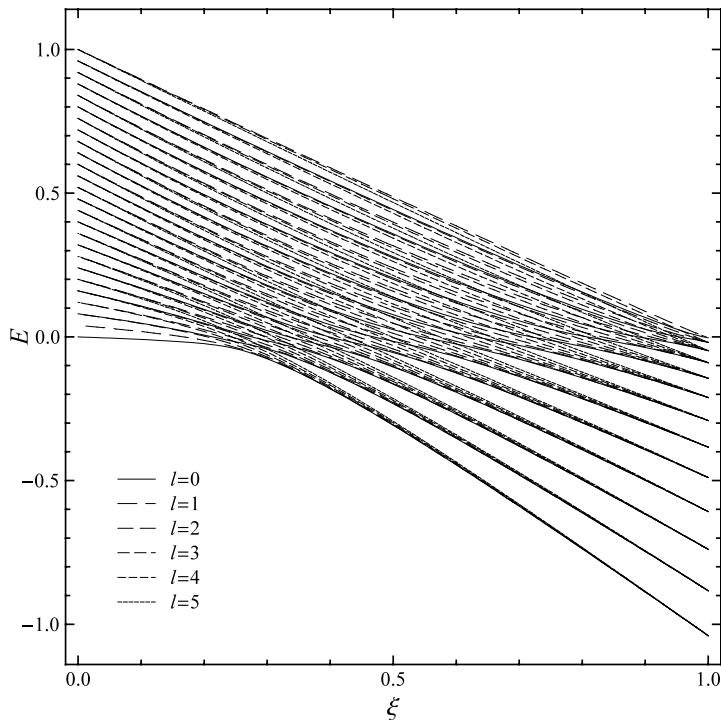
Fig. 10. Correlation diagram for the U(3) vibron model ($N = 25$), with $0 \leqslant l \leqslant 5$, showing the change in angular momentum degeneracies across the ESQPT.

distinction between the states on either side of the QPT lies in their forming approximate embedded representations of either the $U(n_1) \otimes U(n_2)$ or $SO(n_1 + n_2)$ algebras. (In particular, the phases obtained on either side of the ground state QPT have been characterized for the IBM in Ref. [54].) We therefore note that it is of considerable interest to determine whether or not there is a similar sharp distinction between the states, as forming approximate embedded representations of one or the other of these algebras, across the ESQPT.

To consider the question of phases further, let us inspect the structure of the wave functions for the U(3) vibron model excited states, as decomposed in the U(2) (good N_b) dynamical symmetry basis. Each density plot in Fig. 11a–d concisely summarizes the decomposition of the entire spectrum of $l = 0$ eigenstates, for a given value of ξ. [A horizontal slice across the plot gives the "wave function" of one excited state or, more precisely, the squared amplitudes in its decomposition with respect to the U(2) basis. The ground state is represented by the bottommost slice.]

To provide context, first consider the structure of the states when no ESQPT is present. For $\xi = 0$, the Hamiltonian is diagonal in the U(2) basis (Fig. 11a). As ξ increases towards 0.2, the ground state critical value, there is a spreading of the probability distribution over many neighboring basis states, essentially confined to a teardrop shaped region of the N_b–k plot (Fig. 11b). At the other limit, $\xi = 1$, where the SO(3) dynamical symmetry occurs, the probability decomposition also follows a regular pattern (Fig. 11d). Here the wave functions for the eigenstates with respect to the U(2) basis are known analytically
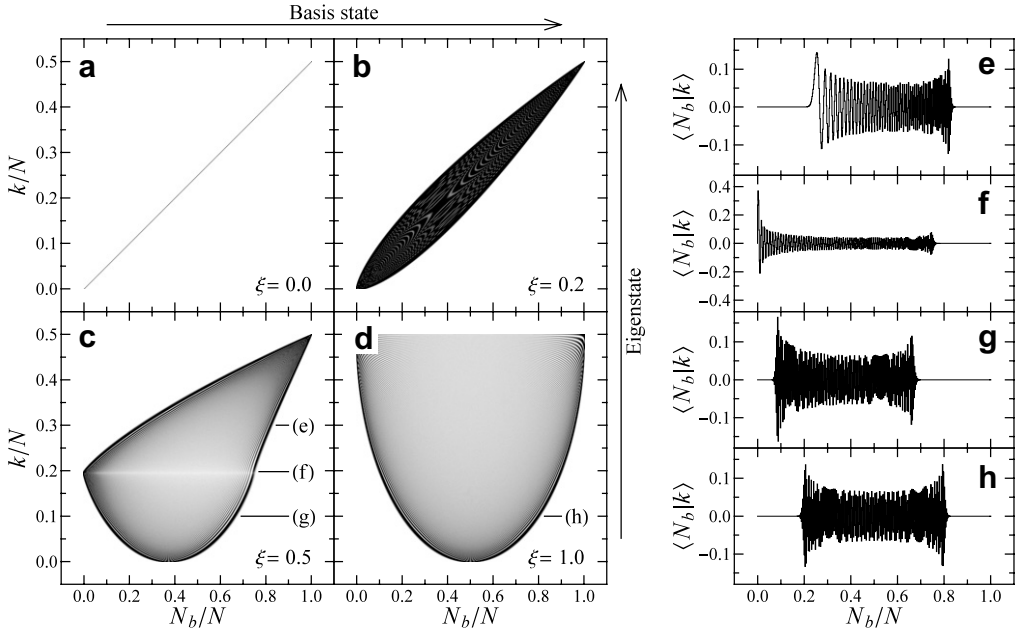
Fig. 11. Probability distributions for the entire spectrum of eigenstates, decomposed with respect to the N_b quantum number, i.e., in the U(2) basis, for the U(3) vibron model with $l = 0$ and $N = 1000$. The probability distributions are shown for (a) $\xi = 0$, (b) $\xi = 0.2$, (c) $\xi = 0.5$, and (d) $\xi = 1$. Also shown are the wave functions for individual representative states: (e) above the ESQPT ($\xi = 0.5$, $k/N = 0.3$), (f) at the ESQPT ($\xi = 0.5$, $k/N = 0.2$), (g) below the ESQPT ($\xi = 0.5$, $k/N = 0.1$), and (h) for the SO(3) dynamical symmetry ($\xi = 1$, $k/N = 0.1$).

[30,55]. The probability distribution for each state is reflection symmetric about $N_b/N = 0.5$, peaked at two symmetric extreme values.

The relevant plot for consideration of the ESQPT is now Fig. 11c, where the probability decompositions of the eigenstates are shown for $\xi = 0.5$. Individual wave functions are shown in Fig. 11e–g, with an SO(3) wave function (Fig. 11h) given for comparison. Below the critical energy ($k/N \approx 0.2$), the probability decompositions, taken in aggregate, bear a marked resemblance to those obtained for the SO(3) dynamical symmetry in Fig. 11d. However, they are scaled towards smaller N_b and, in particular, are approximately reflection symmetric about a reduced value of N_b ($N_b/N \approx 0.4$). In the immediate vicinity of the critical energy, the probability is moderately localized at low N_b. Above the critical energy, the probability distribution for each eigenstate is again strongly peaked at two extreme values of N_b, but these values are not symmetric about a fixed N_b as they are below the critical energy. Rather, their midpoint increases approximately linearly with excitation quantum number, as reflected in the linear behavior of $\langle \hat{N}_b \rangle$ above $E = 0$ in Fig. 7b.

The qualitative distinction between the wave functions below and above the critical energy is therefore clearly apparent when the states are viewed in *aggregate*, as in Fig. 11c. For any given interaction parameter value ξ, the qualitative distinction also apparently involves reflection symmetry (or lack thereof) about some fixed $N_b/N < 0.5$. However, the appropriate means of constructing a simple measure which allows the immediate characterization of the "phase" of a state taken in *isolation* is not obvious and requires further consideration.

6. Conclusions and outlook

In the present work, we have seen that the ESQPT phenomena are universal to a broad family of two-level models with pairing interactions, including not only the s–b models (e.g., Lipkin model, vibron model, and IBM) but also the generic two-level bosonic and fermionic pairing models. The properties of the eigenvalue spectra (including the quantum gap or level density) and order parameters in the vicinity of the ESQPT have been investigated, both at the semiclassical level and numerically for the full quantum problem. The finite-size scaling properties of the gap have been considered at the mean-field level. Qualitative differences between distinct "phases" on either side of the ESQPT have also been noted. In the process, both parallels with and differences from the conventional ground state QPT have been identified.

An important aspect is the experimental evidence for ESQPTs. This requires the identification of physical systems described by algebraic Hamiltonians with $\xi > \xi_c$ for which states with quantum numbers $k \gg 1$ can be observed. The most promising situations thus far are in molecules described by s–b boson models [30]. Further examples are needed to fully understand the experimental implications of the ESQPT.

At the theoretical level, several interesting questions remain even for the basic two-level models considered so far. Here the main intent was to note the aspects of the ESQPT common to the full family of two-level models. A detailed investigation of the specific properties of the bosonic and fermionic two-level models with nontrivial degeneracies for both levels is in order [27]. In particular, an investigation of the $U(n_1 + n_2)/[U(n_1) \otimes U(n_2)]$ geometry of the models is necessary. While the coherent state analysis has been pursued extensively for the s–b models [2,16,38,39,56], only preliminary use of coherent states has so far been made for the generic pairing models [57].

Also, the role of integrability [58] in the ESQPT must be explored. The $SO(n)$-invariant Hamiltonian (2.2), or more generally the $SO(n_1) \otimes SO(n_2)$-invariant or $Sp(n_1) \otimes Sp(n_2)$-invariant Hamiltonian (2.7), is integrable and, moreover, leads to a separable and effectively one-dimensional problem (3.1) in the classical limit. Application of the quantization condition (3.3), which played a crucial role in the semiclassical analysis, is limited to integrable (or approximately integrable) systems. However, interactions beyond the pure pairing interaction are necessary for realistic applications. These interactions destroy integrability. They also in general give rise to *first-order* ground state QPTs, for which even the ground state scaling properties have only been partially characterized [50,59]. Possible manifestation of an ESQPT in the spectrum of a nonintegrable Hamiltonian is discussed in Ref. [60], but a general theoretical foundation for ESQPTs in nonintegrable systems has yet to be developed.

It would be valuable to bridge the gap between the ground state QPT, where the quantum properties scale according to power laws, and the ESQPT, where the singularity is logarithmic in nature. Semiclassically, the connection between the two is nontrivial, since the ground state QPT involves a pure quartic potential (i.e., no barrier) (Fig. 4b), while the ESQPT analysis (Fig. 4c) requires the classical turning point at the barrier to be well-separated from the classical turning point at the outer wall of the well [i.e., a high barrier or, conversely, small $\hbar^2/(2m) \sim 1/N$], so that many states lie below the ESQPT. In actual spectroscopic applications, such as to nuclei, often only relatively few low-lying states can be observed experimentally. Therefore, the finite-N precursors of the ESQPT in the intermediate regime, where the ESQPT is low-lying in the spectrum, are of special interest.

The main physical interest, however, lies in possible broad relevance of the ESQPT phenomena to various mesoscopic systems, at least those dominated by pairing interactions. In this regard, the analysis must be extended to more realistic multi-level pairing models. For instance, the multi-level pairing model with equally spaced levels is of special interest for application to the spectra of superconducting grains [61]. Multi-level pairing models can also provide a foundation for realistic calculations with the nuclear shell model [62]. The models considered in the present work may be constructed as the "infinitely coordinated" limit [49] of the Ising-type spin-lattice models, i.e., the limit in which all sites interact equally with all others by a long-range interaction. It would thus be of interest to examine under what conditions an ESQPT may occur in such models for finite-range interactions. (It has recently been shown [63] that the fermionic two-level pairing Hamiltonian is related to a Bose–Hubbard Hamiltonian [64] by an exact boson mapping, suggesting possible application of the ESQPT concept to correlated electron systems or to ultracold atoms trapped in optical lattices.) An alternate avenue for extension to realistic systems is through coupling of multiple two-level systems as subsystems, e.g., the Dicke model [65] for quantum optical systems may be obtained as two coupled Lipkin models.

Acknowledgments

Appendix A. Quasispin and multipole Hamiltonians for the two-level boson model

The two-level boson model (Fig. 2a) is characterized by two overlaid algebraic structures: a $U(n + 1)$ structure ($n = 2L + 1$) arising from the bilinears in the creation and annihilation operators and an $SU(1, 1)$ structure involving the pairing quasispin operators. The twin algebraic structures provide a simple relationship between the multipole Hamiltonian (2.2) and pairing Hamiltonian (2.3) for the system. In this appendix, we summarize the relevant algebraic properties and deduce the explicit relationship between the pairing and multipole Hamiltonians, for arbitrary L and for the both possible phase choices. The relationship noted for the IBM in Ref. [23] is recovered as a special case.

The well-known bosonic $SU(1, 1)$ quasispin algebra [25] or fermionic $SU(2)$ quasispin algebra [26] generators are given, in the convention we adopt here, by

$$\hat{S}_{j+} \equiv \frac{1}{2} \sum_m c_{jm}^\dagger \tilde{c}_{jm}^\dagger, \quad \hat{S}_{j-} \equiv \frac{1}{2} \sum_m \tilde{c}_{jm} c_{jm}, \quad \hat{S}_{jz} \equiv \frac{1}{4} \sum_m \left(c_{jm}^\dagger \tilde{c}_{jm} + \tilde{c}_{jm} c_{jm}^\dagger \right) \tag{A.1}$$

and obey commutation relations

$$[\hat{S}_{j+}, \hat{S}_{j-}] = \mp 2\hat{S}_{jz}, \quad [\hat{S}_{jz}, \hat{S}_{j+}] = +\hat{S}_{j+}, \quad [\hat{S}_{jz}, \hat{S}_{j-}] = -\hat{S}_{j-}, \tag{A.2}$$

where the upper and lower signs apply to the bosonic and fermionic cases, respectively. The quasispin z projection $\hat{S}_{jz}$ is simply related to the occupancy $\hat{N}_j \equiv \sum_m c_{jm}^\dagger c_{jm}$, by $\hat{S}_{jz} = \frac{1}{2}(\hat{N}_j \pm \Omega_j)$, where Ω_j is the half-degeneracy of level j. The squared quasispin

$$\hat{\mathbf{S}}_j^2 \equiv \hat{S}_{jz}^2 \mp \frac{1}{2}\big(\hat{S}_{j+}\hat{S}_{j-} + \hat{S}_{j-}\hat{S}_{j+}\big) = \hat{S}_{jz}\big(\hat{S}_{jz} - 1\big) \mp \hat{S}_{j+}\hat{S}_{j-}, \tag{A.3}$$

with eigenvalues $\langle\hat{\mathbf{S}}_j^2\rangle = S_j(S_j \mp 1)$, is conserved separately for each level by the Hamiltonian (2.3). Eigenstates are therefore characterized by seniority quantum numbers $v_j = 0, 1, \ldots,$ defined by $S_j = \frac{1}{2}\big(\Omega_j \pm v_j\big)$.

For the two-level bosonic system defined in terms of a singlet level $s^{(0)}$ and an n-fold degenerate level $b^{(L)}$ ($n = 2L + 1$), the quasispin generators (A.1) are given explicitly, in tensor notation, by

$$
\begin{aligned}
\hat{S}_{s+} &= \tfrac{1}{2}(s^\dagger \cdot s^\dagger), & \hat{S}_{b+} &= \tfrac{1}{2}(-)^L\big(b^\dagger \cdot b^\dagger\big) \\
\hat{S}_{s-} &= \tfrac{1}{2}(\tilde{s} \cdot \tilde{s}), & \hat{S}_{b-} &= \tfrac{1}{2}(-)^L(\tilde{b} \cdot \tilde{b}) \\
\hat{S}_{sz} &= \tfrac{1}{4}(s^\dagger \cdot \tilde{s} + \tilde{s} \cdot s^\dagger), & \hat{S}_{bz} &= \tfrac{1}{4}(-)^L\big(b^\dagger \cdot \tilde{b} + \tilde{b} \cdot b^\dagger\big) \\
&= \tfrac{1}{2}\big(\hat{N}_s + \tfrac{1}{2}\big), & &= \tfrac{1}{2}\big(\hat{N}_b + L + \tfrac{1}{2}\big),
\end{aligned}
\tag{A.4}
$$

where $\tilde{T}_\mu^{(\lambda)} \equiv (-)^{\lambda-\mu}T_{-\mu}^{(\lambda)}$ and $U^{(\lambda)} \cdot V^{(\lambda)} \equiv (-)^L(2L+1)^{1/2}(A \times B)^{(0)} = \sum_\mu (-)^\mu U_\mu^{(\lambda)}V_{-\mu}^{(\lambda)}$. The generators of the $SU_s(1,1)$ and $SU_b(1,1)$ algebras can be combined to form a sum-quasispin algebra with two possible relative phases, yielding $SU_\pm(1,1)$ algebras with generators

$$SU_\pm(1,1): \quad \hat{S}_+ = \hat{S}_{s+} \pm \hat{S}_{b+} \quad \hat{S}_- = \hat{S}_{s-} \pm \hat{S}_{b-} \quad \hat{S}_z = \hat{S}_{sz} + \hat{S}_{bz}. \tag{A.5}$$

The subalgebras of $SU_s(1,1) \otimes SU_b(1,1)$, and their associated quantum numbers, are

$$
\underset{\substack{v_s=0,1}}{SU_s(1,1)} \otimes \underset{\substack{v_b}}{SU_b(1,1)} \supset
\begin{cases}
\underset{v_+}{SU_+(1,1)} \\[4pt]
\underset{N_s}{U_s(1)} \otimes \underset{N_b}{U_b(1)} \\[4pt]
\underset{v_-}{SU_-(1,1)}.
\end{cases}
\tag{A.6}
$$

The $SU_s(1,1)$ algebra for the singlet s-boson level is trivial, in that $\hat{\mathbf{S}}^2 = -3/4$ identically by application of the canonical commutation relations for $s_0^\dagger$ and s_0. This constrains v_s to the values 0 or 1. Since $S_z - S$ is integral for $SU(1,1)$ representations, it follows that $v_s = 0$ for N_s even and $v_s = 1$ for N_s odd (i.e., $v_s \cong N_s \bmod 2$).

At fixed total particle number N (and therefore fixed S_z), the operator $\hat{S}_+\hat{S}_-$ is trivially related to the Casimir invariant $\hat{\mathbf{S}}^2$ of $SU_\pm(1,1)$ by (A.3), as $\hat{S}_+\hat{S}_- = S_z(S_z - 1) - \hat{\mathbf{S}}^2$, with eigenvalues $\frac{1}{4}[N(N + 2L) - v_\pm(v_\pm + 2L)]$. A pairing Hamiltonian (2.3) with pairing interaction chosen proportional to the $SU_\pm(1,1)$ Casimir operator is thus given by

$$(\hat{H}_{PP})_\pm = \varepsilon\hat{N}_b + 4\kappa(-)^{L+1}(\hat{S}_{s+} \pm \hat{S}_{b+})(\hat{S}_{s-} \pm \hat{S}_{b-}), \tag{A.7}$$

where the coefficient on the last term is chosen for convenience below.

The two-level boson system is alternatively characterized by the Lie algebra $U(n+1)$, with tensor-coupled generators

$$U(n+1): \quad (s^\dagger \times \tilde{s})^{(0)} \quad (s^\dagger \times \tilde{b})^{(L)} \quad (b^\dagger \times \tilde{s})^{(L)} \quad (b^\dagger \times \tilde{b})^{(\lambda)}, \tag{A.8}$$

for $\lambda = 0, 1, \ldots, 2L$. Two distinct $SO_\pm(n+1)$ subalgebras are obtained, with generators

$$SO_\pm(n+1): \begin{Bmatrix} (s^\dagger \times \tilde{b})^{(L)} + (b^\dagger \times \tilde{s})^{(L)} \\ i[(s^\dagger \times \tilde{b})^{(L)} - (b^\dagger \times \tilde{s})^{(L)}] \end{Bmatrix} \quad (b^\dagger \times \tilde{b})^{(\lambda)}, \tag{A.9}$$

for λ restricted to odd values. In the case of the IBM, it is the $SO_+(6)$ algebra which contains the physical quadrupole operator [66]. [Therefore, conventionally, the $SO_+(6)$ algebra is simply denoted by $SO(6)$, while the alternate $SO_-(6)$ algebra is denoted by $\overline{SO(6)}$.] An n-dimensional rotation algebra $SO(n)$ is obtained by retaining only the generators $(b^\dagger \times \tilde{b})^{(\lambda)}$ (λ odd), and an $SO(3)$ algebra by retaining only $(b^\dagger \times \tilde{b})^{(1)}$ [19].

The subalgebras of $U(n+1)$, and their associated quantum numbers, are thus

$$
\underset{N}{U(n+1)} \supset
\left\{
\begin{array}{c}
\underset{\sigma_+}{SO_+(n+1)} \\[4pt]
\underset{N_s}{U_s(1)} \otimes \underset{N_b}{U(n)} \\[4pt]
\underset{\sigma_-}{SO_-(n+1)}
\end{array}
\right\}
\supset \underset{v}{SO(n)} \supset \underset{J}{SO(3)} .
\tag{A.10}
$$

The Casimir operators of the subalgebras are, explicitly,

$$
C_2[SO_\pm(n+1)] = (\pm)2\left(s^\dagger \times \tilde{b} \pm b^\dagger \times \tilde{s}\right)^{(L)} \cdot \left(s^\dagger \times \tilde{b} \pm b^\dagger \times \tilde{s}\right)^{(L)} + C_2[SO(n)],
$$

$$
C_2[SO(n)] = 4 \sum_{\lambda \text{ odd}} \left(b^\dagger \times \tilde{b}\right)^{(\lambda)} \cdot \left(b^\dagger \times \tilde{b}\right)^{(\lambda)},
$$

$$
C_1[U(n)] = (-)^L \left(b^\dagger \cdot \tilde{b}\right) = \hat{N}_b,
$$

$$
C_2[U(n)] = \sum_\lambda \left(b^\dagger \times \tilde{b}\right)^{(\lambda)} \cdot (b^\dagger \times \tilde{b})^{(\lambda)},
\tag{A.11}
$$

with eigenvalues $2\sigma_\pm(\sigma_\pm + 2L)$, $2v(v + 2L - 1)$, N_b, and $N_b(N_b + 2L)$, respectively. The mathematically natural Casimir form of the Hamiltonian is

$$
(\hat{H}_C)_\pm = \varepsilon N_b + \frac{\kappa}{2} C_2[SO_\pm(n+1)].
\tag{A.12}
$$

The two phase choices for $SO_\pm(n+1)$ yield identical eigenvalue spectra but different eigenstates [66]. For physical reasons, the $SO(n)$-invariant "multipole–multipole" Hamiltonian

$$
\left(\hat{H}_{MM}\right)_\pm = \varepsilon \hat{N}_b + \kappa(\pm)\left[\left(s^\dagger \times \tilde{b} \pm b^\dagger \times \tilde{s}\right)^{(L)} \cdot \left(s^\dagger \times \tilde{b} \pm b^\dagger \times \tilde{s}\right)^{(L)}\right]
\tag{A.13}
$$

is commonly used. At fixed v, $\hat{H}_C$ and $\hat{H}_{MM}$ differ only by a constant offset, with $\left(\hat{H}_{MM}\right)_\pm = \left(\hat{H}_C\right)_\pm - (\kappa/2)C_2[SO(n)]$, by (A.11).

To relate the $U(n+1)$ and $SU(1,1)$ descriptions, let us first observe that the Casimir operators of $SO(n)$ and $SU_b(1,1)$ are related, and that the $SO(n)$ angular momentum quantum number v and the $SU_b(1,1)$ seniority v_b are actually identical. This is an example of a general correspondence between the algebras $SO(n)$ and $SU(1,1)$ [67,68]. According to the basic quasispin relations above,

$$
4\hat{\mathbf{S}}_b^2 = \left(\hat{N}_b + L + \frac{1}{2}\right)\left(\hat{N}_b + L - \frac{3}{2}\right) - 4\hat{S}_{b+}\hat{S}_{b-},
\tag{A.14}
$$

and $4\hat{S}_{b+}\hat{S}_{b-} = (b^\dagger \cdot b^\dagger)(\tilde{b} \cdot \tilde{b})$ can be recast in terms of coupled bilinears in the creation and annihilation operators (e.g., by the tensor contraction methods of Ref. [69]) as

$$
4\hat{S}_{b+}\hat{S}_{b-} = (-)^{L+1}\left(b^\dagger \cdot \tilde{b}\right) + \sum_\lambda (-)^\lambda \left(b^\dagger \times \tilde{b}\right)^{(\lambda)} \cdot \left(b^\dagger \times \tilde{b}\right)^{(\lambda)}.
\tag{A.15}
$$

The right hand side we reexpress in terms of the Casimir operators (A.11) as

$$4\hat{S}_{b+}\hat{S}_{b-} = -\hat{N}_b + C_2[\mathrm{U}(n)] - \frac{1}{2}C_2[\mathrm{SO}(n)]. \tag{A.16}$$

On the other hand, $\langle 4\hat{S}^2 \rangle = \left(v_b + 2L + \frac{1}{2}\right)\left(v_b + 2L - \frac{3}{2}\right)$ from the definition of seniority. Comparison with the result for $\langle 4\hat{S}^2 \rangle$ obtained from (A.14) and (A.16) establishes the identity of v and v_b.

Comparison of the full Hamiltonians $\hat{H}_{\mathrm{PP}}$ (A.7) and $\hat{H}_{\mathrm{MM}}$ (A.13) is then straightforward, with the aid of (A.16), yielding

$$\left(\hat{H}_{\mathrm{MM}}\right)_{\pm} = \left(\hat{H}_{\mathrm{PP}}\right)_{[\mp(-)^L]} + \kappa(-)^L[N(N+2L) - v(v+2L-1)]. \tag{A.17}$$

Thus, for L even, the Hamiltonians $\left(\hat{H}_{\mathrm{MM}}\right)_{\pm}$ and $\left(\hat{H}_{\mathrm{PP}}\right)_{\mp}$ differ only by a constant (i.e., a function of conserved quantum numbers), while, for L odd, it is $\left(\hat{H}_{\mathrm{MM}}\right)_{\pm}$ and $\left(\hat{H}_{\mathrm{PP}}\right)_{\pm}$ which differ only by a constant. Observe, therefore, that for the U(2), U(6), etc., models (L even), the conventional $\mathrm{SU}_+(1,1)$ phase choice for the *pairing* interaction ($G_{ij} = 1$) corresponds to the unconventional $\mathrm{SO}_-(n+1)$, or $\overline{\mathrm{SO}(n+1)}$, phase choice for the *multipole* interaction, and *vice versa*.

Finally, let us consider how the general $\mathrm{U}(n+1)$ scheme (A.10) specializes to the Schwinger realization of the Lipkin model ($L = 0$). With the usual Schwinger angular momentum operator definitions $J_+ = b^\dagger s$, $J_- = s^\dagger b$, and $J_z = \frac{1}{2}(b^\dagger b - s^\dagger s)$, the subalgebra structure is

$$\mathrm{U}(2) \supset \underset{J=\frac{1}{2}N}{\mathrm{SU}(2)} \supset \begin{cases} \underset{J_x}{\mathrm{SO}_+(2)} \equiv \mathrm{SO}_x(2) \\ \underset{J_z=\frac{1}{2}(N_b-N_s)}{\mathrm{U}(1)} \equiv \mathrm{SO}_z(2) \\ \underset{J_y}{\mathrm{SO}_-(2)} \equiv \mathrm{SO}_y(2). \end{cases} \tag{A.18}$$

The breaking of $\mathrm{U}(n)$ into $\mathrm{SO}_+(n+1)$, $\mathrm{SO}_-(n+1)$, and $\mathrm{U}(n)$ subalgebras therefore has a particularly simple interpretation, as the projection of the SU(2) angular momentum alternatively along the x, y, or z axes.

Furthermore, both the s and b bosonic levels are singlet levels in the Lipkin model. It follows, as already noted for the s boson in (A.6), that the seniorities v_s and v_b are restricted to the values 0 or 1, with $v_s \cong N_s \bmod 2$ and $v_b \cong N_b \bmod 2$. Thus, the grading quantum number g defined in Section 4.1, which determines the Lipkin model parity $\pi = (-)^g$, is simply the $\mathrm{SU}_b(1,1)$ quasispin seniority v_b. This formally explains the similarity, discussed in Section 4.1, between the role of g in the Lipkin model and that of the $\mathrm{SO}(n)$ angular momentum in the higher-dimensional s–b algebras (Fig. 6a and b). However, for the Lipkin model ($n = 1$), there is no $\mathrm{SO}(n)$ angular momentum dual to the $\mathrm{SU}_b(1,1)$ seniority.

Appendix B. The Lambert W function

The Lambert W function [70] is implicitly defined as the solution $y = W(x)$ to the equation
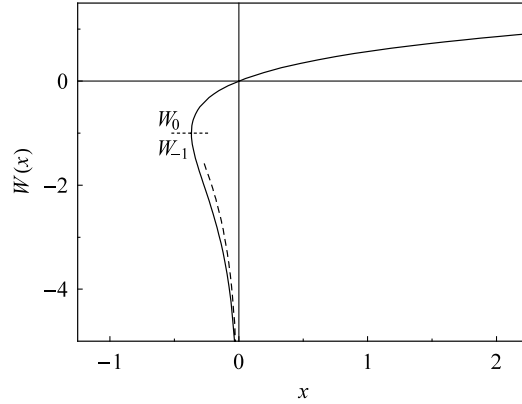
$$x = ye^y. \tag{B.1}$$

Fig. B.1. The Lambert W function. For $-1/e < x < 0$, $W(x)$ is double-valued, with branches $W_0(x) \geqslant -1$ and $W_{-1}(x) \leqslant -1$. The asymptotic form of $W_{-1}(x)$ given by (B.2) is shown for comparison (dashed line).

In this appendix, we summarize the essential properties of the W function needed for the present analysis (Section 3). The complex analysis, asymptotics, series expansion, etc., of the W function are considered in detail in Ref. [70].

Considered as a real-valued function of a real variable, $W(x)$ is single-valued for $x \geqslant 0$ but double-valued for $-1/e < x < 0$, with branches $W_0(x) \geqslant -1$ and $W_{-1}(x) \leqslant -1$. These branches are plotted in Fig. B.1. The function has the asymptotic form [70,71]

$$W_{-1}(x) \sim \log(-x) - \log[-\log(-x)] \tag{B.2}$$

as $x \to 0^-$, shown as the dashed curve in Fig. B.1.

From the defining Eq. (B.1), it follows that W obeys the identity

$$\log W(x) = \log x - W(x). \tag{B.3}$$

Differentiation yields

$$W'(x) = \frac{W(x)}{x[1 + W(x)]}. \tag{B.4}$$

It also follows from (B.1) that the equation

$$y \log y + cy = x \tag{B.5}$$

has solution $y = x/W(e^c x)$, as needed for Section 3.3.

References

[1] R. Gilmore, D.H. Feng, Nucl. Phys. A 301 (1978) 189.
[2] D.H. Feng, R. Gilmore, S.R. Deans, Phys. Rev. C 23 (1981) 1254.
[3] M. Vojta, Rep. Prog. Phys. 66 (2003) 2069.
[4] W.D. Heiss, M. Müller, Phys. Rev. E 66 (2002) 016217.
[5] W.D. Heiss, F.G. Scholtz, H.B. Geyer, J. Phys. A 38 (2005) 1843.
[6] F. Leyvraz, W.D. Heiss, Phys. Rev. Lett. 95 (2005) 050402.
[7] S. Heinze, P. Cejnar, J. Jolie, M. Macek, Phys. Rev. C 73 (2006) 014306.
[8] M. Macek, P. Cejnar, J. Jolie, S. Heinze, Phys. Rev. C 73 (2006) 014307.
[9] P. Cejnar, M. Macek, S. Heinze, J. Jolie, J. Dobeš, J. Phys. A 39 (2006) L515.

[10] W.D. Heiss, J. Phys. A 39 (2006) 10081.
[11] H.J. Lipkin, N. Meshkov, A.J. Glick, Nucl. Phys. 62 (1965) 188.
[12] F. Iachello, A. Arima, The Interacting Boson Model, Cambridge University Press, Cambridge, 1987.
[13] R.P. Feynman, Phys. Rev. 56 (1939) 340.
[14] M.E. Fisher, M.N. Barber, Phys. Rev. Lett. 28 (1972) 1516.
[15] A.E.L. Dieperink, O. Scholten, F. Iachello, Phys. Rev. Lett. 44 (1980) 1747.
[16] A.E.L. Dieperink, O. Scholten, Nucl. Phys. A 346 (1980) 125.
[17] O.S. Van Roosmalen, Ph.D. thesis, Rijksuniversiteit Groningen, 1982.
[18] F. Iachello, R.D. Levine, Algebraic Theory of Molecules, Oxford University Press, Oxford, 1995.
[19] F. Iachello, Lie Algebras and Applications, Lecture Notes in Physics, vol. 708, Springer, Berlin, 2006.
[20] J.M. Arias, J. Dukelsky, J.E. García-Ramos, J. Vidal, Phys. Rev. C 75 (2006) 014301.
[21] P. Cejnar, F. Iachello, J. Phys. A 40 (2007) 581.
[22] R.A. Broglia, C. Riedel, B. Sørensen, Nucl. Phys. A 107 (1968) 1.
[23] A. Arima, F. Iachello, Ann. Phys. (NY) 123 (1979) 468.
[24] F. Pan, J.P. Draayer, Nucl. Phys. A 636 (1998) 156.
[25] H. Ui, Ann. Phys. (NY) 49 (1968) 69.
[26] A.K. Kerman, Ann. Phys. (NY) 12 (1961) 300.
[27] M.A. Caprio, F. Iachello, in preparation.
[28] F. Iachello, S. Oss, J. Chem. Phys. 104 (1996) 6956.
[29] F. Pérez-Bernal, L.F. Santos, P.H. Vaccaro, F. Iachello, Chem. Phys. Lett. 414 (2005) 398.
[30] F. Pérez-Bernal, F. Iachello, in preparation.
[31] R. Gilmore, Lie Groups, Lie Algebras, and Some of Their Applications, Wiley, New York, 1974.
[32] W. Zhang, D.H. Feng, R. Gilmore, Rev. Mod. Phys. 62 (1990) 867.
[33] M.S. Child, J. Phys. A 31 (1998) 657.
[34] K.W. Ford, D.L. Hill, M. Wakano, J.A. Wheeler, Ann. Phys. (NY) 7 (1959) 239.
[35] J.R. Cary, P. Rusu, R.T. Skodje, Phys. Rev. Lett. 58 (1987) 292.
[36] J.R. Cary, P. Rusu, Phys. Rev. A 45 (1992) 8501.
[37] J.R. Cary, P. Rusu, Phys. Rev. A 47 (1993) 2496.
[38] J.N. Ginocchio, M.W. Kirson, Nucl. Phys. A 350 (1980) 31.
[39] R.L. Hatch, S. Levit, Phys. Rev. C 25 (1982) 614.
[40] A. Messiah, Quantum Mechanics, Dover, Mineola, New York, 1999.
[41] I.S. Gradshteyn, I.M. Ryzhik, Table of Integrals, Series, and Products, 5th ed., Academic Press, Boston, 1994.
[42] M. Abramowitz, I.A. Stegun, Handbook of Mathematical Functions, Dover, New York, 1965.
[43] K.-E. Thylwe, S. Yngve, P.O. Fröman, J. Math. Phys. 47 (2006) 073510.
[44] S. Dusuel, J. Vidal, J.M. Arias, J. Dukelsky, J.E. García-Ramos, Phys. Rev. C 72 (2005) 011301R.
[45] N. Fröman, P.O. Fröman, Physical Problems Solved by the Phase-Integral Method, Cambridge University Press, Cambridge, 2002.
[46] J.L. Tennyson, J.R. Cary, D.F. Escande, Phys. Rev. Lett. 56 (1986) 2117.
[47] J.R. Cary, D.F. Escande, J.L. Tennyson, Phys. Rev. A 34 (1986) 4256.
[48] R.N. Dixon, Trans. Faraday Soc. 60 (1964) 1363.
[49] R. Botet, R. Jullien, Phys. Rev. B 28 (1983) 3955.
[50] D.J. Rowe, P.S. Turner, G. Rosensteel, Phys. Rev. Lett. 93 (2004) 232502.
[51] S. Dusuel, J. Vidal, Phys. Rev. B 71 (2005) 224420.
[52] S. Dusuel, J. Vidal, Phys. Rev. A 71 (2005) 060304.
[53] J. Carvalho, R.L. Blanc, M. Vassanji, D.J. Rowe, J.B. McGrory, Nucl. Phys. A 452 (1986) 240.
[54] D.J. Rowe, Nucl. Phys. A 745 (2004) 47.
[55] E. Santopinto, R. Bijker, F. Iachello, J. Math. Phys. 37 (1996) 2674.
[56] A. Leviatan, Ann. Phys. (NY) 179 (1987) 201.
[57] H. Chen, T. Song, D.J. Rowe, Nucl. Phys. A 582 (1995) 181.
[58] M. Tabor, Chaos and Integrability in Nonlinear Dynamics: An Introduction, Wiley, New York, 1989.
[59] F. Iachello, N.V. Zamfir, Phys. Rev. Lett. 92 (2004) 212501.
[60] M. Macek, P. Stránský, P. Cejnar, S. Heinze, J. Jolie, J. Dobeš, Phys. Rev. C 75 (2007) 064318.
[61] J. von Delft, D.C. Ralph, Phys. Rep. 345 (2001) 61.
[62] A. Volya, B.A. Brown, V. Zelevinsky, Phys. Lett. B 509 (2001) 37.
[63] F. Pan, J.P. Draayer, 2007, available from nucl-th/0703007.

[64] J. Hubbard, Proc. R. Soc. Lond. A 276 (1963) 238.
[65] R.H. Dicke, Phys. Rev. 93 (1953) 99.
[66] P. Van Isacker, A. Frank, J. Dukelsky, Phys. Rev. C 31 (1985) 671.
[67] F. Pan, Y.-F. Cao, J. Math. Phys. 29 (1988) 2384.
[68] D.J. Rowe, J. Phys. A 38 (2005) 10181.
[69] J.-Q. Chen, B.-Q. Chen, A. Klein, Nucl. Phys. A 554 (1993) 61.
[70] R.M. Corless, G.H. Gonnet, D.E.G. Hare, D.J. Jeffrey, D.E. Knuth, Adv. Comput. Math. 5 (1996) 329.
[71] N.G. de Bruijn, Asymptotic Methods in Analysis, Bibliotheca mathematica, vol. 4, Second ed., North-Holland, Amsterdam, 1961.